

Preparation, Characterization and Dye/Heavy Metal Adsorption Properties of Bio-based Composites

Akeem Adeyemi Oladipo

Submitted to the
Institute of Graduate Studies and Research
in partial fulfillment of the requirements for the degree of

Doctor of Philosophy
in
Chemistry

Eastern Mediterranean University
September 2015
Gazimağusa, North Cyprus

Approval of the Institute of Graduate Studies and Research

Prof. Dr. Serhan Ciftcioglu
Acting Director

I certify that this thesis satisfies the requirements as a thesis for the degree of Doctor of Philosophy in Chemistry.

Prof. Dr. Mustafa Halilsoy
Chair, Department of Chemistry

We certify that we have read this thesis and that in our opinion it is fully adequate in scope and quality as a thesis for the degree of Doctor of Philosophy in Chemistry.

Assoc. Prof. Dr. Mustafa Gazi
Supervisor

Examining Committee

1. Prof. Dr. Ayfer Saraç
2. Prof. Dr. Bahire Filiz Şenkal
3. Prof. Dr. Osman Yilmaz
4. Assoc. Prof. Dr. Mustafa Gazi
5. Assoc. Prof. Dr. Rana Kidak

ABSTRACT

Biomagnetic composite based on raw *Ferula communis* and polyacrylamide (MBFC) was synthesized. The MBFC proved to be an effective and high performance adsorbent for the removal of heavy metals, acidic and basic dyes from simulated effluents by batch and fixed-bed experiments. The morphology, surface and magnetic properties of the as-prepared MBFC were examined by Boehm titration; scanning electron microscope and Fourier transform infrared techniques. The sorption process was optimized via Box-Behnken approach and techno-economic analysis completed using central composite design.

The adsorption isotherm, kinetics and parametric behaviors of the pollutants were investigated, and detailed explanation of the results is discussed. The maximum removal efficiencies of the pollutants of 69.3–96.9% were obtained at the optimum operation conditions of 50 mgL⁻¹ initial adsorbate concentration, 100 mg MBFC dose, 360 min contact time, pH 4.0 (acidic dyes) and pH 7.0 (basic dyes and heavy metal ions). The rate-controlling mechanism is discussed in terms of intraparticle diffusion, and the actual step was confirmed by Boyd model. Finally, the efficiency and stability of MBFC were assessed via several regeneration-reuse cycles.

Keywords: Bio-based composite; acid dyes; basic dyes; heavy metals; adsorption optimization; modeling; thermokinetic studies.

ÖZ

Ham Ferula communis ve poliakrilamid esaslı biyomanyetik kompozit (MBFC) sentezlenmiştir. MBFC'nin batch ve sabit yatak deneyleriyle ağır metaller, asidik ve bazik boyaların simule atıklarından giderimi için etkili ve yüksek performanslı bir adsorbent olduğu kanıtlandı. Hazırlanmış MBFC'nin morfolojisi, yüzey ve manyetik özellikleri Boehm titrasyonu; taramalı elektron mikroskobu ve Fourier kızılötesi dönüşüm teknikleri ile incelenmiştir. Sorpsiyon süreci Box-Behnken yaklaşımı ile optimize edilmiş ve merkezi kompozit tasarım kullanarak tekno-ekonomik analizi tamamlanmıştır.

Adsorpsiyon izotermi, kinetik ve kirletici parametrik davranışlar araştırıldı ve sonuçların detaylı açıklamaları tartışılmıştır. Kirleticiler için maksimum giderim etkinliği, 50 mgL⁻¹ başlangıç adsorbat konsantrasyonu, 100 mg MBFC dozunda 360 dakika temas süresi, pH 4,0 (asidik boyalar) ve pH 7.0 (bazik boya ve ağır metal iyonları) optimum çalışma koşullarında % 69.3–96.9 olarak belirlenmiştir. Oran-kontrol mekanizması partikül içi difüzyon açısından ele alınmış ve gerçek aşama Boyd modeli ile teyit edilmiştir. Son olarak, MBFC'nin etkinliği ve stabilitesi birçok rejenerasyon-yeniden döngüleri ile değerlendirilmiştir.

Anahtar Kelimeler: Biyo-bazlı kompozit; asidik boyalar; bazik boyalar; ağır metaller; adsorpsiyon optimizasyon; modelleme; termokinetik çalışma.

ACKNOWLEDGEMENT

To my supervisor, if I had to choose between thanking you and praising you I would rather look back in time and say you are a great person that allows me to fly even without wings. Thank you sir!

My wholehearted appreciation to the jury members who diligently took the time to read and provided insightful suggestions and comments that aided the completion of this study. Yes to my parents and sibs!.....I have done it again, you guys words of encouragement, prayer and support channeled me to the successful paths. Kudos!

Hey Mr. Bandy-Leg Ayo and my Iranian blond Melika, thank you guys for providing me the distractions that I sporadically needed during the lab sessions and around my cute office....I appreciate the friendship!....and seeing you guys in the labs has been such an unforgettable experience. To Mosab, thanks man for the friendship.!

My profound appreciation goes to Prof. Elvan and Asst. Prof. Mehmet G. for keeping me on track and... sincere gratitude to Dr. Kivanc for being patient and simple during my teaching assistantship days!

TABLE OF CONTENTS

ABSTRACT.....	iii
ÖZ.....	iv
ACKNOWLEDGEMENT.....	v
LIST OF TABLES.....	viii
LIST OF FIGURES.....	ix
LIST OF SCHEMES.....	xi
LIST OF SYMBOLS.....	xii
1 INTRODUCTION.....	1
1.1 Thesis Objectives.....	3
1.2 Scope of Study.....	3
1.3 Thesis Structure.....	4
2 LITERATURE REVIEW.....	6
2.1 General Information.....	6
2.2 Types of Pollutants in Nature.....	6
2.2.1 Heavy Metals.....	7
2.2.2 Dyes.....	10
2.3 Pollutant Removal Technique: Adsorption Process.....	12
2.4 Modeling and Optimization by Response Surface Methodology.....	14
3 EXPERIMENTAL.....	16
3.1 Materials and Reagents.....	16
3.2 Preparation of Adsorbates.....	16
3.3 Preparation of Adsorbents.....	17
3.3.1 Preparation of Activated Carbon from Pre-washed <i>F.communis</i>	18
3.3.2 Preparation of Biomagnetic composite.....	19

3.3.3 Preparation of Magnetic Activated Carbon-based Composite.....	20
3.3.4 Preparation of Biopolymeric Composites	20
3.3.5 Preparation of Magnetic Biopolymeric Hybrid Composites.....	21
3.4 Characterization of Adsorbents	22
3.5 Experimental Adsorption Process	23
3.6 Data Evaluation, Optimization, and Modeling.....	24
3.7 Isotherm, Kinetic and Thermodynamic Studies	26
3.8 Desorption Experiments and Spent Adsorbents Reuse	28
4 RESULTS AND DISCUSSION	30
4.1 Introduction	30
4.2 Characterization	31
4.3 Results of Optimization Studies and Statistical Analysis	33
4.4 Effects of Independent Variables on Adsorbates Removal.....	43
4.4.1 Batch Studies.....	43
4.4.2 Fixed-bed Studies.....	52
4.5 Equilibrium Isotherm, Kinetics, and Sorption Thermodynamics	60
4.6 Regeneration and Reuse Results	70
5 CONCLUSION	73
REFERENCES	75

LIST OF TABLES

Table 1: Heavy metals toxicities and sources	8
Table 2: Methods for treatment of heavy metal containing wastewaters	9
Table 3: Classification of dyes and some discussions	11
Table 4: Physicochemical properties and chemical structure of dyes used in this study	17
Table 5: Experimental design for MBFC and levels of process factors	26
Table 6: Linear forms of isotherm equations and short description of the models....	27
Table 7: Kinetic equations and short description of the models	28
Table 8: Details of adsorbents synthesized and pollutants removed	30
Table 9: Physicochemical properties of the synthesized adsorbents	32
Table 10: BBD experimental design for dye removal using MBFC	33
Table 11: BBD experimental design for heavy metal removal using MBFC	34
Table 12: ANOVA from BBD for removal of heavy metal/dye using MBFC.....	35
Table 13: Experimental design by CCD for heavy metal and dye removal using MBFC	41
Table 14: The isotherms parameters in single component system	61
Table 15: Isotherm parameters for binary component system.....	62
Table 16: Pseudo-first and pseudo-second-order kinetic parameters	65
Table 17: Parameters for intraparticle diffusion and Boyd mechanism.....	66
Table 18: Thermodynamic parameters in single and binary systems	70

LIST OF FIGURES

Figure 1: Types of pollutants in nature	7
Figure 2: Differences and similarities between dyes and pigments.....	10
Figure 3: Typical adsorption process	13
Figure 4: Common and emerging adsorbents	14
Figure 5: Pre-treated <i>F.communis</i> adsorbents (a) dried at 12 h (b) dried at 24 h	18
Figure 6: Activated carbon prepared from <i>F.communis</i> (FC-AC)	19
Figure 7: Pictorial representation of the raw and biomagnetic composite.....	20
Figure 8: Synthesis pathway for magnetic hybrid composite and pictorial representation	22
Figure 9: Response surface plots showing the interactive effects of pH and contact time	37
Figure 10: Response surface plots showing the effects of concentration and dosage	38
Figure 11: Effect of pH for acidic and cationic dyes removal by various adsorbents	44
Figure 12: Effect of solution pH on the removal of cationic dyes by various adsorbents	45
Figure 13: (a) Simulations of copper ion speciation and sorption by adsorbents	46
Figure 14: Effect of (a) MBFC and (b) FC dosage on heavy metal removal	48
Figure 15: Variation in adsorption of (a) Cu and (b) Ni by MBFC as a function of pH and foreign cations.....	50
Figure 16: Variation in adsorption of (a) Cv and (b) Rh cationic dyes by MBFC as a function of pH and foreign cations	51
Figure 17: Effect of bed depths on acidic dyes adsorption by MBFC.....	53
Figure 18: Influence of bed depth on the removal of cationic dyes by MBFC.....	54

Figure 19: Effect of bed depth on copper removal by MBFC	55
Figure 20: Effect of bed depth on nickel and zinc removal by MBFC	56
Figure 21: Effect of bed depth on manganese removal in bed column of MBFC	57
Figure 22: Effect of flow rate on dye removal in bed column of MBFC	59
Figure 23: Plot of intraparticle diffusion of dyes and heavy metal ions	67
Figure 24: Boyd plots for Dr80 and Cu ²⁺ removal by MBFC.....	68
Figure 25: Desorption of loaded MBFC using different desorbing agents at 298K..	71
Figure 26: Reusability of MBFC	72

LIST OF SCHEMES

Scheme 1: Illustration of magnetic separation of pollutants from simulated effluent	31
Scheme 2: Schematic illustration of synergistic adsorption between nickel-loaded adsorbent and acid red 25.....	64

LIST OF SYMBOLS

C_i	Initial dye concentration (mg/L)
C_e	Concentration at equilibrium (mg/L)
C	Intraparticle diffusion model constant
k_1	Pseudo-first order kinetic rate constant (1/min)
k_2	Pseudo-second order kinetic rate constant (g/mg min)
K_L	Langmuir adsorption constant (L/g)
K_F	Freundlich adsorption constant (L/g)
K_s	Sips biosorption constant (L/g)
k_d	Intraparticle rate constant (mg/gmin ^{0.5})
n	Freundlich constant
q_e	Amount adsorbed onto adsorbent at equilibrium (mg/g)
q_t	Amount of dye adsorbed at time t (mg/g)
$q_{e,cal}$	Calculated amount adsorbed at equilibrium (mg/g)
$q_{e,exp}$	Experimental amount of dye adsorbed at equilibrium (mg/g)
q_m	Maximum adsorption capacity for adsorbent (mg/g)
R^2	Correlation coefficient
T	Absolute temperature (K)
Greek Factors	
β_{ii}	Quadratic effect in Box-Behnken model
β_{ij}	Interaction effect in Box-Behnken model
ε	Polanyi potential

Chapter 1

INTRODUCTION

Nowadays organic and inorganic pollutants are present in wastewaters of photographic processing factories, wineries, plastics, pigments, metal plating, mining, tanneries, textile and leather industries ([Hameed and El-khaiary, 2008](#); [Pandiselvi and Thambidurai, 2013](#)). The presence of these pollutants has been increasingly recognized as a serious threat to health if their limit overshoots tolerable amount in drinking or usable water. In fact, these pollutants are not only detestable to aesthetic sense inducing ecological damages but also, their recalcitrant nature are of great concern to the public and environmental scientists ([Imamoglu, 2013](#); [Khosa et al., 2011](#)).

Effluents of the above-mentioned industries generally contain portions of dyes and heavy metals including copper (Cu), nickel (Ni), zinc (Zn), arsenic (As), chromium (Cr), lead (Pb), and mercury (Hg). The dyes are intensely colored, reduce dissolved oxygen, contain multicomponent organic-inorganic structure, and annihilate aquatic life ([Oladipo et al., 2014](#); [Pandiselvi and Thambidurai, 2013](#)). Also, most of these heavy metals are released to the environment in amounts that are perilous to the environment due to increase in their prevalence, acute toxicity, and persistence within the environment ([Acharya et al., 2009](#)).

Among these heavy metals, Cr, Se, As, Pb, Cd, and Hg are routinely listed at the top on the toxicity list. However, the common heavy metals such as Ni, Cu, and Zn are vital elements when in small quantities for various lives, but are potentially fatal when the tolerable limits are exceeded (Demirbas, 2008; Wang and Chen, 2014). As reported in the literature (Sezgin et al., 2013), copper even in low quantity generates toxic effects in living organisms because it produces oxygen-rich species that can destroy proteins, nucleic acids, and lipids (Oladipo and Gazi, 2015a). Excessive nickel can also cause various health problems including diarrhea, lung irritation, paralysis, renal damage, and bone malformation (Oladipo and Gazi, 2014a). The maximum allowable concentrations recommended by health and environmental protection authorities differ from region to region, however commonly reported limits, sources and toxicity of some metal ions are given in Table 1.

Heavy metal ions and ionic dyes frequently co-exist in industrial effluents constituting the most recalcitrant environmental pollution. Therefore, there is a compelling interest to develop viable, economic, and efficient treatment technologies that can not only clean-up but also degrade the pollutants under ambient operating conditions. A number of methods have been reported for removal of these co-pollutant; however, some of these methods suffer from various limitations such as high investment costs, low regenerability of the materials used, generation of concentrated sludge/toxic wastes and low selectivity (Farooq et al., 2010; Oladipo et al., 2014; Sezgin et al., 2013). Thus, there is a steadfast search for an optimal treatment method while considering its investment cost, efficiency and sources of materials used and removal capacity.

1.1 Thesis Objectives

The objective of this study is to remove ionic dyes and heavy metals from wastewater using environmentally stable, bio-based, economic and recyclable materials. The specific goals of the project are:

- To develop high-performance bio-based composites for wastewater treatment
- To evaluate the efficiency and selectivity of the prepared composites in batch and fixed-bed sorption systems
- To systematically model the treatment factors and obtain the optimal operating conditions
- To assess the selectivity of the prepared composite in the presence of multi-pollutants
- To establish the mechanism of removal of the studied pollutants using the prepared composites
- To minimize the operation costs

1.2 Scope of Study

As stated, this thesis focused on wastewater treatment using various synthesized bio-based composites for the removal of heavy metals (nickel, copper, manganese and zinc) and ionic dyes (acid red 25, rhodamine b, crystal violet and direct red 80). The wastewater was simulated artificially in the lab. The bio-based composites were tested for removal of single pollutant and multi-pollutants in both batch and fixed-bed systems.

The bio-based composites were thoroughly characterized, and the analyte concentrations were determined using UV–VIS spectrophotometer (Beijing, T80+) under ambient conditions. Adsorption experiments were conducted in triplicate to

estimate the reliability of the results and average results were reported in all cases. Fixed-bed experiments were conducted in a glass column packed with wool at both layers in similar conditions with batch studies. The investigated parameters were optimized to obtain highest removal efficiency via central composite design, and Box-Behnken models. Additionally, regeneration and reusability of spent adsorbents were evaluated, and various thermo-kinetic models were applied to explain the removal mechanisms.

1.3 Thesis Structure

The thesis report is divided into the following chapters:

Chapter One introduces the problem statement, the background of the project, and the necessity of this research.

Chapter Two explores preliminary studies reported by other researchers. This chapter introduces the need for low-cost bio-based adsorbents, emphasizes the advantages of removing the investigated pollutants via adsorption technique and difficulties faced in treating wastewater containing multi-pollutants.

Chapter Three discusses the experimental techniques employed to achieve the desired objectives of this study. It presents tests that were performed including the procedures, equipment used, and relevant information regarding the experiments.

Chapter Four discusses the results obtained and explained observations during the experiments both unfavorable and favorable and scenarios. The chapter highlights optimal operation conditions that lead to the most efficient removal capacity, as well

as fitting the experimental data to various models. Additionally, the results obtained from regeneration and reusability of spent adsorbents was also discussed here.

Chapter Five highlights the outcomes obtained from this research and provides an overall conclusion to the thesis including recommendations.

Chapter 2

LITERATURE REVIEW

2.1 General Information

The freshwater scarcity and the increasingly presence of refractory contaminants, particularly in agricultural and industrial wastewaters, are resulting in strict environmental regulations. Of these contaminants, heavy metals and dyes have received much recognition because of their detrimental and toxic effects when present in large quantities (Deng et al., 2013). Over twenty heavy metals and fifty dye types have been considered harmful, and roughly half of these numbers are discharged to the environment in amounts that are dangerous to human health and the environment (Mohammad et al., 2009; Oladipo and Gazi, 2015b).

2.2 Types of Pollutants in Nature

Over the years, pollution has been recognized as remarkable challenges facing the environment. The quantity of potentially toxic substances released into the ecosystem increases as the world's population grows. In basic definition, a pollutant is regarded as energy or any substances that adversely affects or possess undesired effects on the usefulness of a resource, when introduced into the environment. Broadly, pollutants can be classified into three main groups as indicated in Fig. 1.

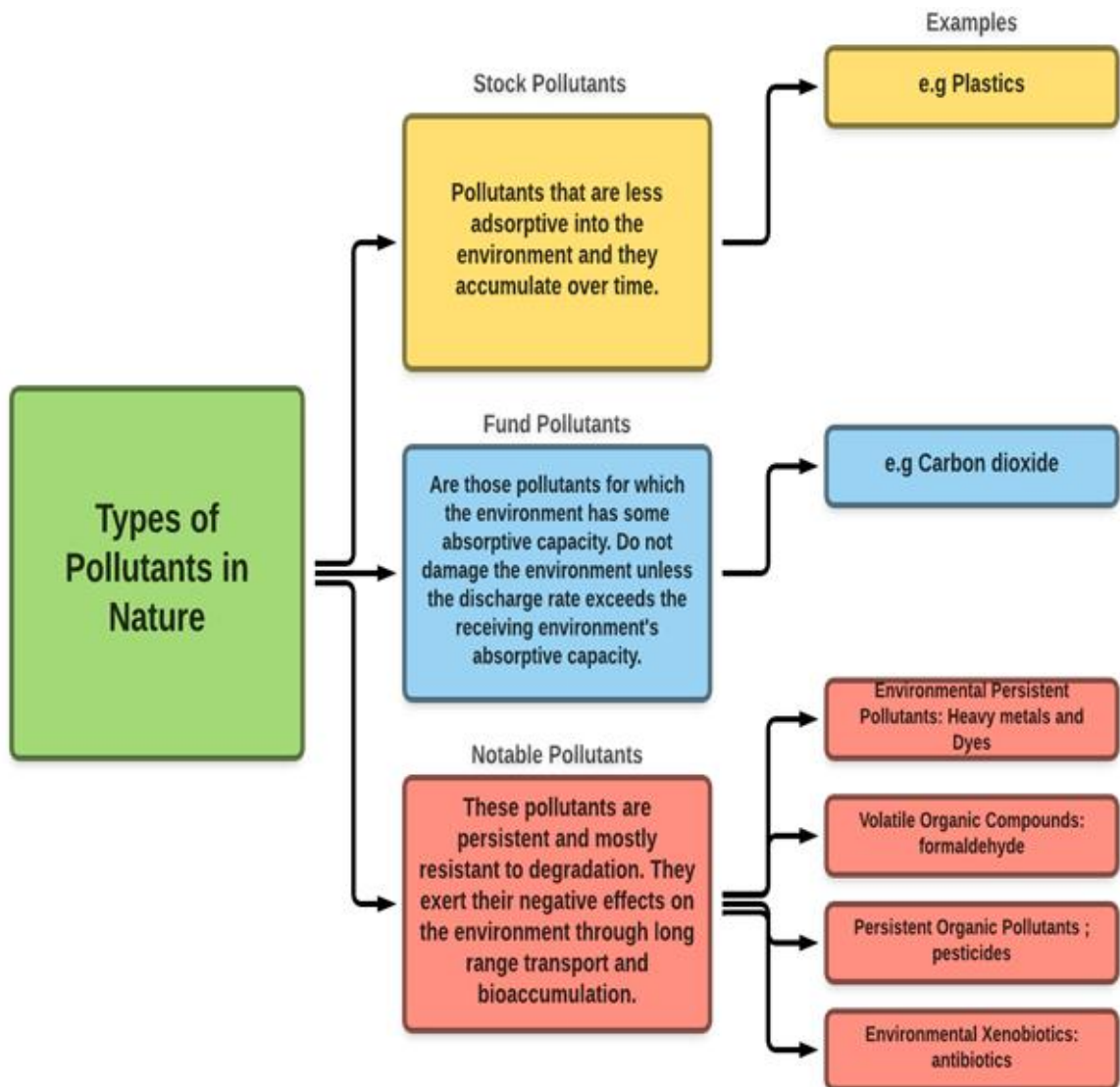


Figure 1: Types of pollutants in nature

This research work focused majorly on the removal of environmentally persistent pollutants (heavy metals and dyes).

2.2.1 Heavy Metals

The phrase “heavy metals” (viz. Cu, Zn, Ni, Mn etc.) refers to metals that are relatively dense and potentially toxic or poisonous even at lower concentrations (Farooq et al., 2010). They are mostly present as traces within the earth’s crust and difficult to neither eliminate nor degrade. However, traces of some of these metals (zinc, copper, selenium, and iron) play essential metabolic role within the body

system while higher amounts results to poisoning (Demirbas, 2008; Kang et al., 2010; Oladipo and Gazi, 2015a). Heavy metals are continuously discharge into the environment via anthropogenic sources, and these toxic metals enhance contamination of rural, industrial and urban wastewaters. Hence, their presence is of significant concern to the general populace due to their carcinogenic and non-degradable behavior (Farooq et al., 2010, Oladipo and Gazi, 2015c). The toxicity and sources of some metal ions are given in Table 1.

Table 1: Heavy metals toxicities and sources

	Heavy metals			
	Copper	Zinc	Nickel	Manganese
Toxicities	Neurotoxicity, dizziness, developmental and reproductive toxicity.	Gastrointestinal distress, diarrhea, nausea and causes “metal-fume fever”.	Lung cancer, low blood pressure, acute bronchitis and decreased lung function.	Parkinson's disease, Epigastric pain nausea and neurotoxic effects.
Sources	Mining, copper polishing, printed circuit board production, wood Preservatives & paint production.	Manufacturing processes and mining works.	Mineral processing, Porcelain enameling, & paint formulation.	Batteries production, coal mining, forest fires, mineral and mining processing.
Limits (mgL ⁻¹)	0.25 ^a	0.80 ^a	0.02 ^d – 0.2 ^a	0.1 ^c – 0.4 ^b
References	Oladipo and Gazi, 2015; Kang et al., 2010	Farooq et al., 2010	Saeed et al., 2005; Oladipo and Gazi, 2014	Idris, 2015; Zhang et al., 2014

Source: a: USEPA, b: WHO, c: Chinese Regulatory body d: European Union

The metal-containing effluents if discharged directly into the sewage system will seriously harm aquatic species and unsuitable for agricultural activities. Hence, due to the toxicity of heavy metals-laden wastewaters, it is necessary that industrial

effluents are treated completely or the concentration of pollutants reduced to acceptable limits before being discharged into water streams. Some methods have been reported to treat heavy metal containing effluents, and [Table 2](#) compares some of these methods.

Table 2: Methods for treatment of heavy metal containing wastewaters

Treatment methods	Advantages	Limitations
Electrochemical methods	<ul style="list-style-type: none"> • Heavy metal selective • Pure metals can be obtained • No consumption of chemicals/reagents 	<ul style="list-style-type: none"> • High investment cost • Strict solution pH and Current density • High running cost
Ultrafiltration and Membrane process	<ul style="list-style-type: none"> • Less sludge produced • High efficiency for single metal ion • Less chemical consumption 	<ul style="list-style-type: none"> • High running cost • Removal (%) reduces in the presence of other metal ions • Low flow rates
Chemical coagulation	<ul style="list-style-type: none"> • Sludge dewatering • Sludge settling 	<ul style="list-style-type: none"> • High initial cost • High consumption of chemicals
Ion-exchange	<ul style="list-style-type: none"> • High selectivity • High regeneration of spent materials 	<ul style="list-style-type: none"> • High recovery cost • Less number of metal ions removed
Adsorption: activated carbon	<ul style="list-style-type: none"> • High efficiency (>98%) • Most heavy metals can be removed 	<ul style="list-style-type: none"> • Poor regeneration • Cost of activated carbon • Performance depends upon source of material
Adsorption: clay and biomass	<ul style="list-style-type: none"> • Most metals can be removed • Relatively less expensive materials 	<ul style="list-style-type: none"> • Low removal efficiency • Poor selectivity • Separation difficulty after used

Source: (Farooq et al., 2010)

2.2.2 Dyes

Dyes and pigments are powerful colorants and conventionally applied to improve the material aesthetic character. They do so because they absorb certain wavelengths of light preferably. Dyes are mostly soluble in aqueous solution and have an affinity for the substrate; however, pigments are mainly insoluble with no affinity to the substrate. Some of the differences and similarities between dyes and pigments are depicted in Fig.2.

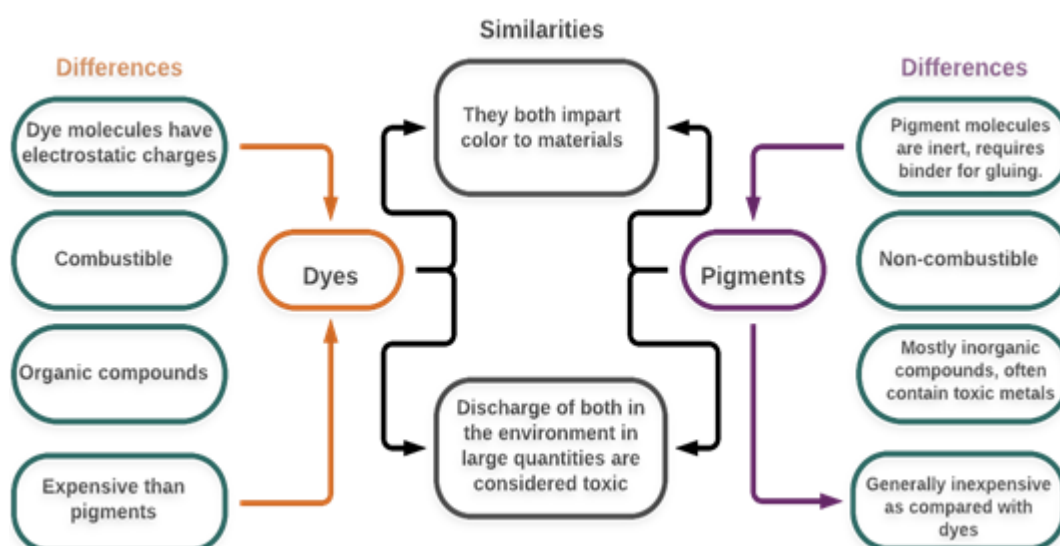


Figure 2: Differences and similarities between dyes and pigments

Around 50,000 –73,000 tons of commercial dyes are produced annually worldwide, and the higher percentages are concentrated in industrial nations (Oladipo et al., 2015; Zhang et al., 2011). The increasing dye production is due to a variety of technological applications of dyes in textile, leather, plastic, paper and food industries. The textile factories are considered one of the highest water-consuming spheres. Thus, during and after the technological processes, nearly 15% of the dyes are lost into aquatic streams (Duran et al., 2008; Yan et al., 2014). Many of these dyes are considered toxic to aquatic life; even tiny quantity in water may cause

obvious color change and in addition, the effluents containing various colored dyes may cause some ecological issues (Zhao et al., 2012). In general, dye-containing effluents are characterized by their high color, total organic carbon (TOC), biological oxygen demand (BOD), total dissolved solid (TDS), and chemical oxygen demand (COD). Dyes can be classified according to their structures, their applications or methods of application on the substrate. Table 3 shows some of the characteristics of dye types.

Table 3: Classification of dyes and some discussions

Classification of dyes	Specific information
Acid dyes	<ul style="list-style-type: none"> • Acid dyes contain water-soluble anionic moieties that are applied to the fiber in acid and neutral dye-baths. • They can induce sensitization primarily due to their molecular structure and mode of metabolism. • Due to their complex aromatic structure, they are considered toxic, and their usage is restricted.
Basic dyes	<ul style="list-style-type: none"> • These are water-soluble cationic dyes, applied majorly to acrylic fibers • Acetic acid is frequently added to the dye-bath to improve the basic dye uptake to the fiber.
Reactive dyes	<ul style="list-style-type: none"> • Consist of chromophore as a substituent to directly react with the substrate. • The reaction occurs via covalent bonds between reactive dye molecules and fibers to give permanent color. • They are prime choice for dyeing cellulose and cotton fiber
Mordant dyes	<ul style="list-style-type: none"> • It requires a mordant (potassium dichromate) to improve its fastness against light, perspiration and water. • Contains at least 30% of dyes and applied mostly on navy shades and black. • Heavy metal-based mordant are considered hazardous to health, and extreme care must be taken in using them.

2.3 Pollutant Removal Technique: Adsorption Process

Various techniques and methods have been utilized to remove pollutants from water streams or industrial effluents. Some of these techniques have shown a remarkable success. However, they suffer from various limitations such as cost, selectivity, low removal efficiency, and regeneration. Within, adsorption process is utilized and discussed due to its advantages over other known reported techniques.

The adsorption process is thought to have been applied centuries ago; however, the first observations or results were documented around 1700's ([Dabrowski, 1999](#)). During the mentioned period, adsorption was specifically utilized to investigate the potential of charcoals, clays, rocks and sands to uptake different gasses. After extensive research, de Saussure in 1814 concluded that all gasses can be adsorbed by any porous materials in addition to materials mentioned above ([Ruthven, 1984](#); [Manal, 2009](#)). During the early 1900s, various adsorption models and equations were developed to predict the monolayer and multilayer sorption mechanisms including the Freundlich, Euckena, Langmuir, Polanyi and Brunauer-Emmett-Teller (BET) equations ([Manal, 2009](#)).

Adsorption is a process of collecting dissolved substances (adsorbates) from aqueous solutions on the surface of the materials (adsorbents) being used. “Absorption process” involves collection of adsorbates over the whole volume of the absorbing materials, while “adsorption process” is surface-based phenomenon similar to surface tension as shown in [Fig.3 \(Oladipo et al., 2014\)](#).

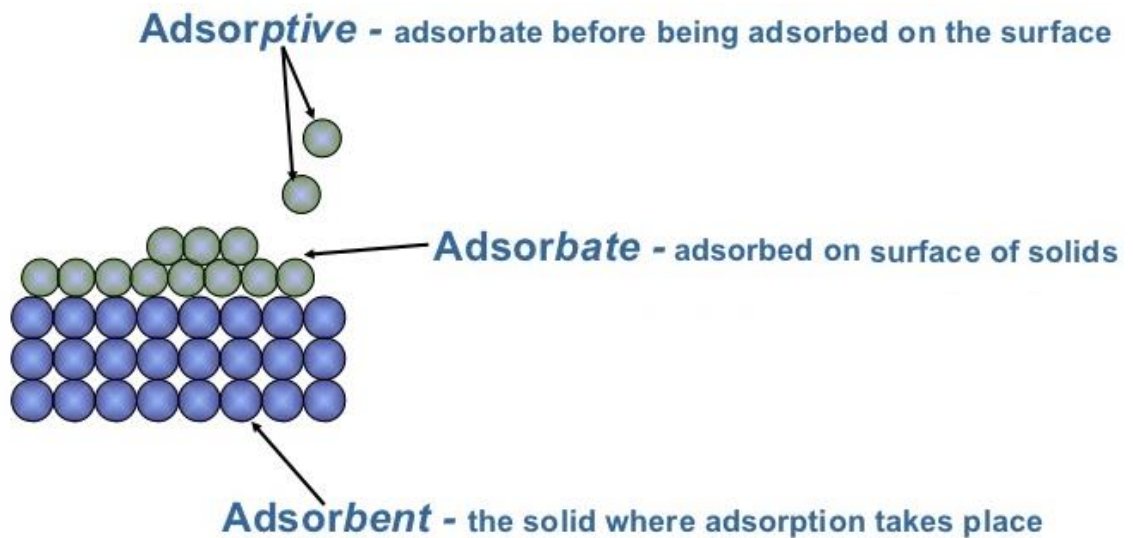


Figure 3: Typical adsorption process

During the adsorption process, the atoms or ions from the adsorbates within the surface of the adsorbents are not surrounded by other adsorbents atoms or ions, and thus interaction between the adsorbent surface and adsorbates occur. In adsorption process, the nature of bonding depends on the nature of the species involved. Hence, sorption process may be via weak van der Waals forces (physisorption), sometimes takes place due to the electrostatic attraction (ion-exchange) or covalent bonding (chemisorption).

Over the years, various kinds of materials have been applied to adsorb dissolved inorganics and organics in industrial wastewater, drinking water, domestic wastewater, seawater among other classes of water sources. Each of the water types has varying dissolved substances according to source, location, application of the water, thresholds and the codes of the government. Varying results are also obtained from the treatment and purification processes based on the wastewater, nature of dissolved substances and methods utilized (Manal, 2009). Solubility plays significant role in adsorption process; since the more hydrophilic the dissolved substances, the

less their ability to be adsorbed while the more hydrophobic the substance, the greater its ability to be adsorbed (Dabrowski, 1999). In addition to adsorption, other forms of removal technique may take place simultaneously such as precipitation or degradation. However, it is beyond the scope of this research to estimate the quantity of pollutant (heavy metals) removed by adsorption and those removed via precipitation. Some of the common and emerging adsorbents are shown in Fig. 4.

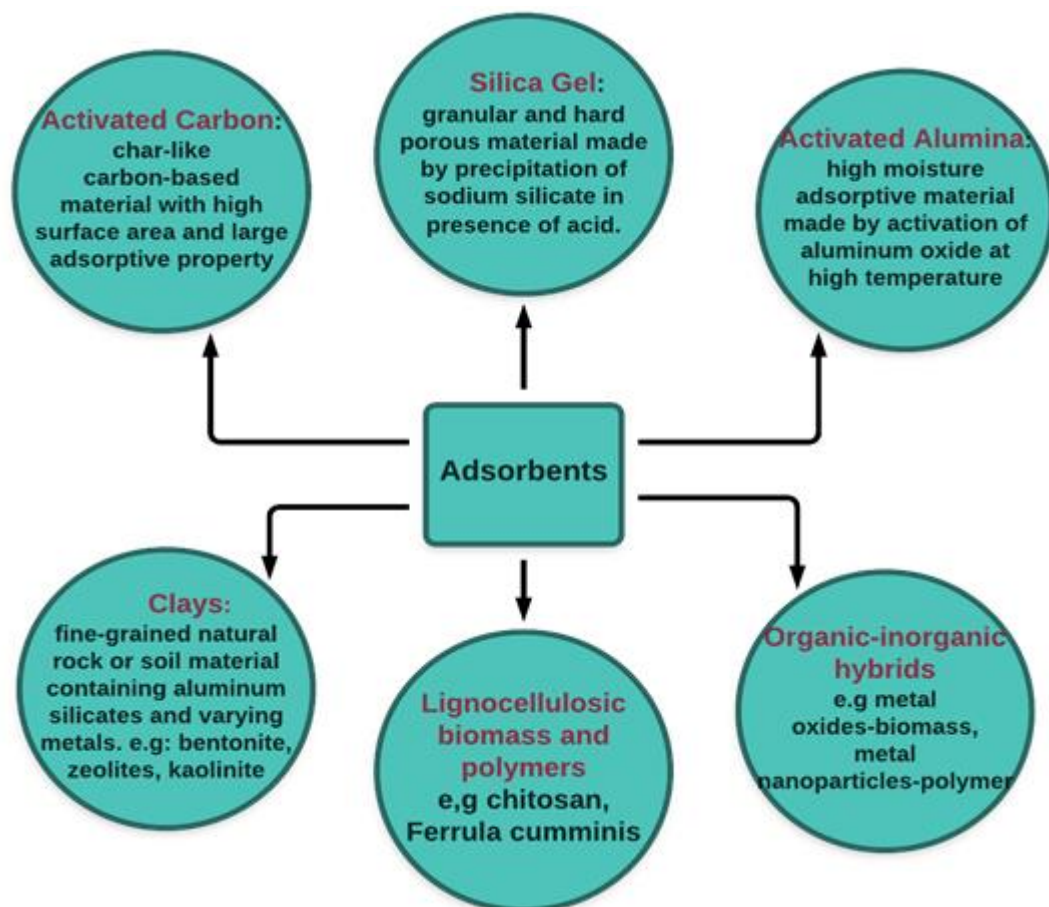


Figure 4: Common and emerging adsorbents

2.4 Modeling and Optimization by Response Surface Methodology

Response surface methodology (RSM) is a distinct set of statistical and mathematical methods applicable for designing experiments, studying the effect of various factors

affecting the response and optimizing the adsorption parameters (Oladipo and Gazi, 2015abc; Cui et al., 2015). As compared with the conventional system of designing experiments, RSM reduces the number of operating variables by taking into account only important factors. Hence, RSM enhances process performance, reduces time consumption and overall operation costs (Asfaram et al., 2015).

Various researchers have reported that total experimental time was reduced, and optimum operating parameters were established when RSM was applied as compared to the time consuming conventional technique of designing adsorption process. For instance, Oladipo et al. (2015c) applied RSM to estimate and predict competitive adsorption between azo and anthraquinone dyes, obtained results established the optimum factors influencing binary mixture of azo and anthraquinone dyes in a timely manner. Similarly, Cui et al. (2015) were able to predict and optimize effectively interactive factors between Pb (II) and methylene. Hence, two RSM models (central composite design and Box-Behnken methodology) were applied in this research to estimate the significant factors affecting single and multicomponent adsorption process and to explain the competitive effects of multi-components in the simulated wastewater.

Here, stems of *Ferula communis* (çakşır otu) were utilized as biomass support. The *Ferula communis* (the giant fennel) is a species in the genus *Ferula* of the Apiaceae and belongs to genus *Foeniculum*. *Ferula communis* is a tall herbaceous perennial. It is found in Mediterranean and East African woodlands and shrublands (Seki et al. 2013).

Chapter 3

EXPERIMENTAL

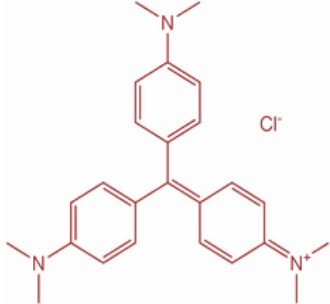

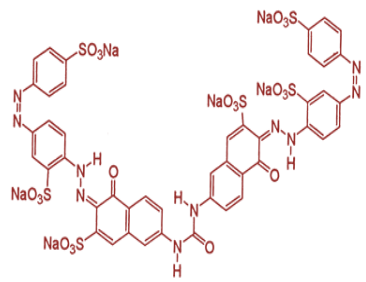
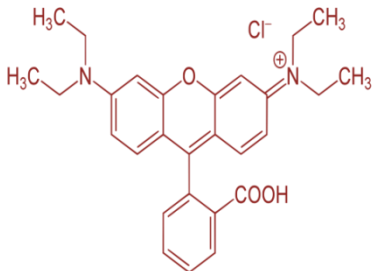
3.1 Materials and Reagents

Analytical grade reagents were used throughout without purification. Stems of *Ferula communis* were collected from Pergamos regional area of North Cyprus. Iron (II) sulfate heptahydrate, copper (II) nitrate trihydrate, glutaraldehyde, and sodium hydroxide were purchased from Fluka (Switzerland). Also, N, N'-methylene-bis-acrylamide (MBA), acrylamide (AAM), hydrochloric acid (HCl) and zinc chloride (ZnCl_2) were utilized and purchased from Merck (Germany). Solutions were prepared by dissolving precisely weighed samples of materials in distilled water to obtain the required concentration.

3.2 Preparation of Adsorbates

Stock solutions (1000 mgL^{-1}) of heavy metals (Cu, Zn, Ni and Mn) and dyes (crystal violet, acid red 25, direct red 80 and rhodamine **b**) were prepared by dissolving pre-calculated amount of the metal salts and pure dye compounds respectively in distilled water. The working solutions for the sorption experiments were freshly prepared from the stock solutions via serial dilutions until desired concentration ($20 - 500 \text{ mgL}^{-1}$) obtained. For each adsorbate, a calibration curve was plotted, and necessary working data were extracted. The physicochemical characteristics of the dyes are shown in [Table 4](#).

Table 4: Physicochemical properties and chemical structure of dyes used in this study

Name	Chemical structures	Dye types	Molar mass (gmol ⁻¹) & Color index number	λ_{\max} (nm)
Crystal violet (Cv) Cationic dye		Type: Triarylmethane Solubility (%): water 0.2-1.8, acetone 0.4 and ethanol 3.0-14.0	407.97 C.I. 42555	590.00
Acid red 25 (Ar25) Anionic dye		Type: Single-azo class Solubility (%): water 0.3-2.3, acetone 0.3 and ethanol 2.5-12.0	502.43 C.I. 16050	508.00
Direct red 80 (Dr80) Anionic dye		Type: Multi-azo class Solubility (%): water 0.1-1.3, ethanol 0.5-0.15 Moreover, insoluble in most organic solvents	1373.08 C.I. 35780	528.00
Rhodamine b (Rb) Cationic dye		Type: Fluorescence tetraethyl class Solubility (%): water 0.1-1.5, ethanol 5-9, acetic acid 400	479.01 C.I. 45170	554.00

3.3 Preparation of Adsorbents

The sun-dried *F.communis* stems were washed in tap water to remove dirt and coloring materials. Then, soaked in distilled water for 5 h and repeatedly washed

until the clear filtrate was observed. The washed *F.communis* was dried at 60 – 100 °C in an oven for 12 – 24 h, crushed to a fine grain-like powder using ball mill (Fisher, Loughborough, UK), and sieved to obtain particles at a size < 200 μm. The obtained powder was labeled FC and utilized as starting material for preparation of various composites as presented in Fig. 5.

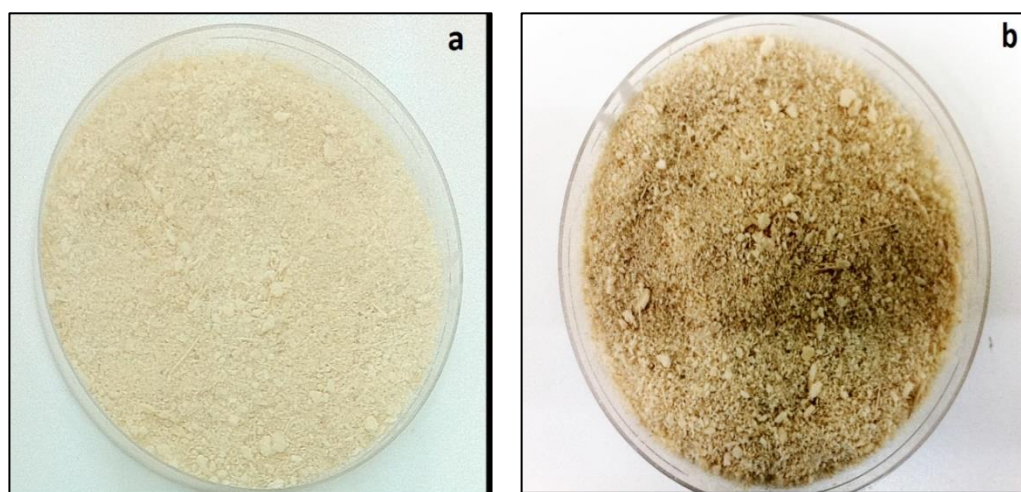


Figure 5: Pre-treated *F.communis* adsorbents (a) dried at 12 h (b) dried at 24 h

3.3.1 Preparation of Activated Carbon from Pre-washed *F.communis*

Activated carbon was prepared and described in detail in our previous work (Oladipo and Gazi, 2015a). In brief, accurately weighed sample of FC (20 g) was soaked in $ZnCl_2$ (0.73 mol) solution for 24 h at 70 °C. After the chemical activation of the precursor by $ZnCl_2$ (activating agent/FC= 60%), the activated FC was collected, dried overnight and then transferred into a muffle furnace for carbonization. The activated FC was heated ($10\text{ }^\circ\text{Cmin}^{-1}$) for 60 min to final carbonization temperature (600 °C). The carbonized product was washed several times with HCl (0.5 N), hot water and finally in distilled water to remove mineral matters, organic and residual Zn. The activated carbon was dried in conventional oven dried at 110 °C for 4 h, and

then crushed to a fine powder in a small ball mill and labeled FC-AC for experimental use as shown in [Fig. 6](#).

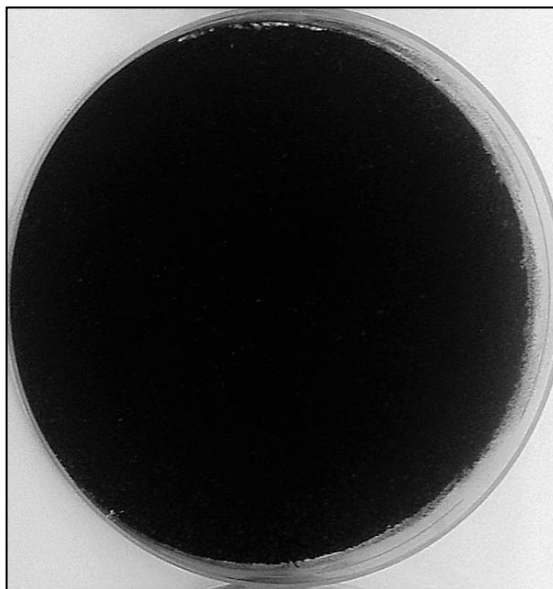


Figure 6: Activated carbon prepared from *F. communis* (FC-AC)

3.3.2 Preparation of Biomagnetic composite

The biomagnetic composite was prepared by co-precipitation of ferrite particles and FC in the presence of sodium hydroxide under thermal treatment as described in our previous paper ([Oladipo and Gazi, 2015b](#)). In brief, solutions of copper nitrate (0.02 mol) and ferrous sulfate (0.036 mol) were thoroughly mixed in 200 mL Erlenmeyer flask (Fe/Cu: mole ratio 2/1), precise amount of FC was added to above mixture under constant stirring at 90 °C and, then sodium hydroxide (75.0 mmol) was introduced slowly until brownish-black precipitate obtained. The biomagnetic composite obtained was separated by an external magnet, washed sequentially with ethanol and distilled water, and finally dried in an oven at 100 °C for 24 h. The biomagnetic composite was cooled to room temperature and labeled MFC for experimental use as shown in [Fig. 7](#).

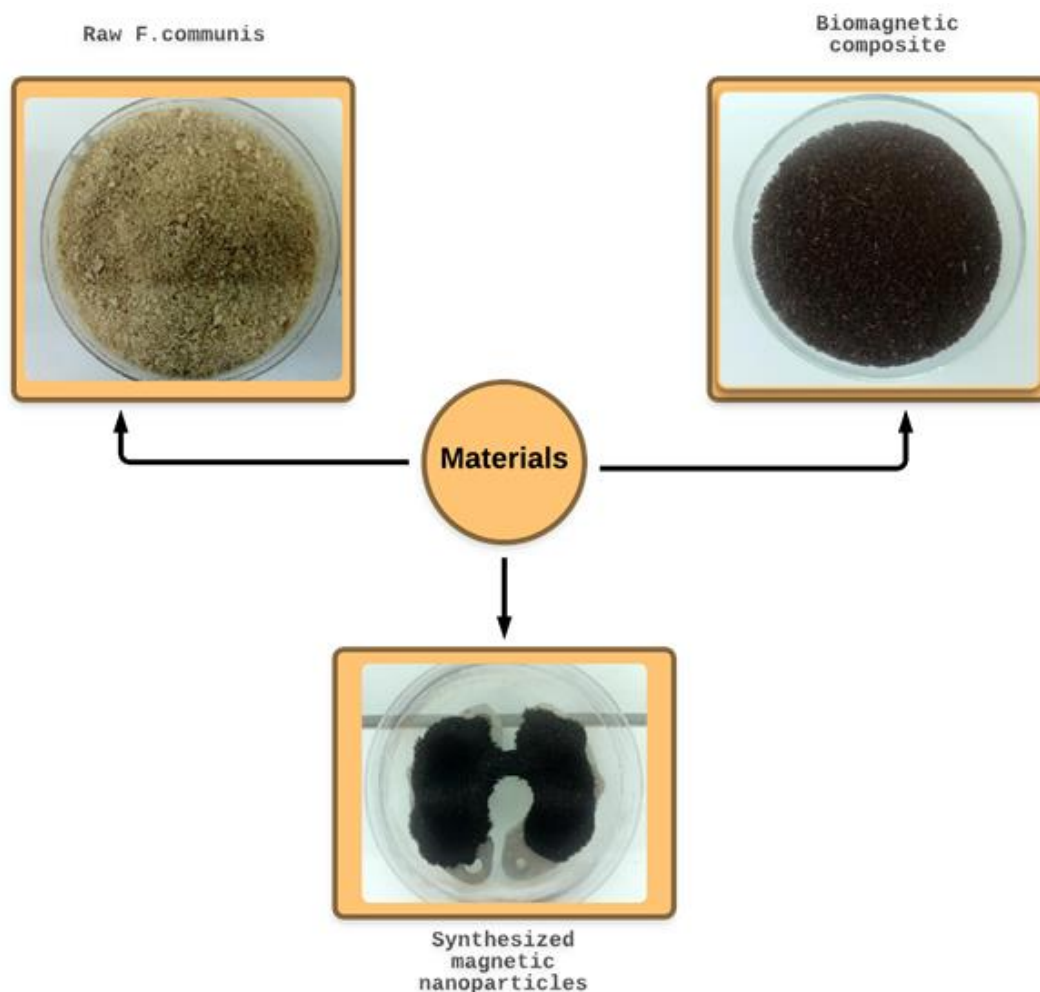


Figure 7: Pictorial representation of the raw and biomagnetic composite

3.3.3 Preparation of Magnetic Activated Carbon-based Composite

The magnetic activated carbon was prepared similarly as biomagnetic composite, however, earlier prepared (sec.3.3.1) activated was used as the starting material instead of FC. Briefly, known amount of FC-AC was added to a solution of copper and iron salts under constant stirring. The final product was obtained by dropwise precipitation using sodium hydroxide solution, dried and labeled as MFAC.

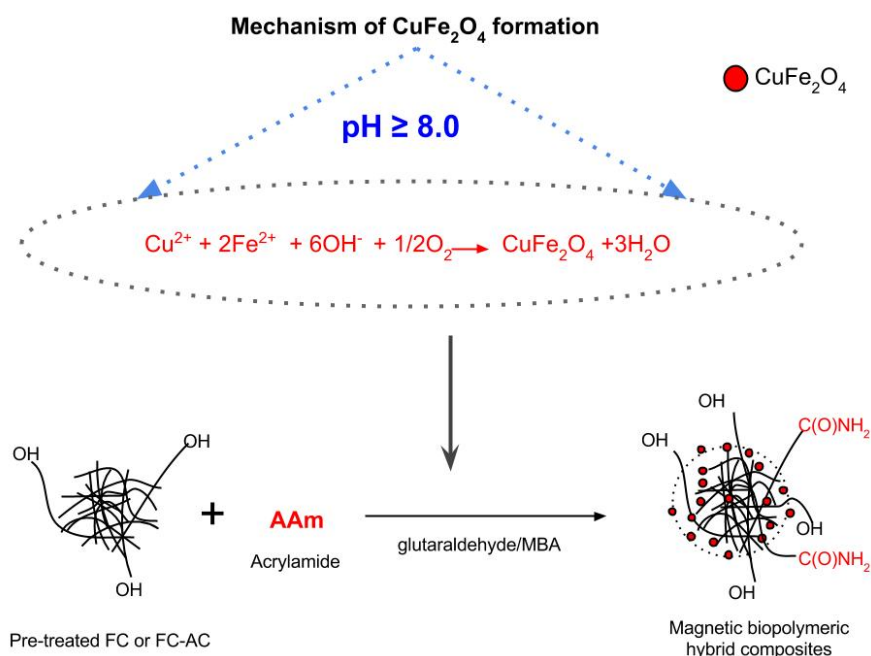
3.3.4 Preparation of Biopolymeric Composites

Biopolymeric composites containing FC and FC-AC were prepared and reported in [Oladipo and Gazi \(2015a\)](#). In brief, a pre-weighed amount of FC or FC-AC (50% of total product weight) was added to solutions of acrylamide (0.84 mol) in two

different Erlenmeyer flasks (300 mL) equipped with thermometer and stirred for 4 h under nitrogen. Then, the mixtures were irradiated for 5 min in a domestic microwave oven (Saatchi: NL-MO-6128D, 1200 W) in the presence of 1.2 g of MBA (cross-linker). Obtained biopolymeric composites were repeatedly washed in acetone and distilled water to remove unreacted materials, then dried at ambient condition for 8 h, and labeled as PFC and PFCAC respectively for adsorption studies.

3.3.5 Preparation of Magnetic Biopolymeric Hybrid Composites

The preparation of magnetic biopolymeric hybrid composites (MBFC and MBAC) was achieved by a combination of ferrite formation, encapsulation and chemical crosslinking processes (Oladipo and Gazi, 2015ab; Oladipo et al., 2015). A brief illustration of the synthesis of magnetic biopolymeric hybrid composites and pictorial representation of final products is shown in Fig. 8.



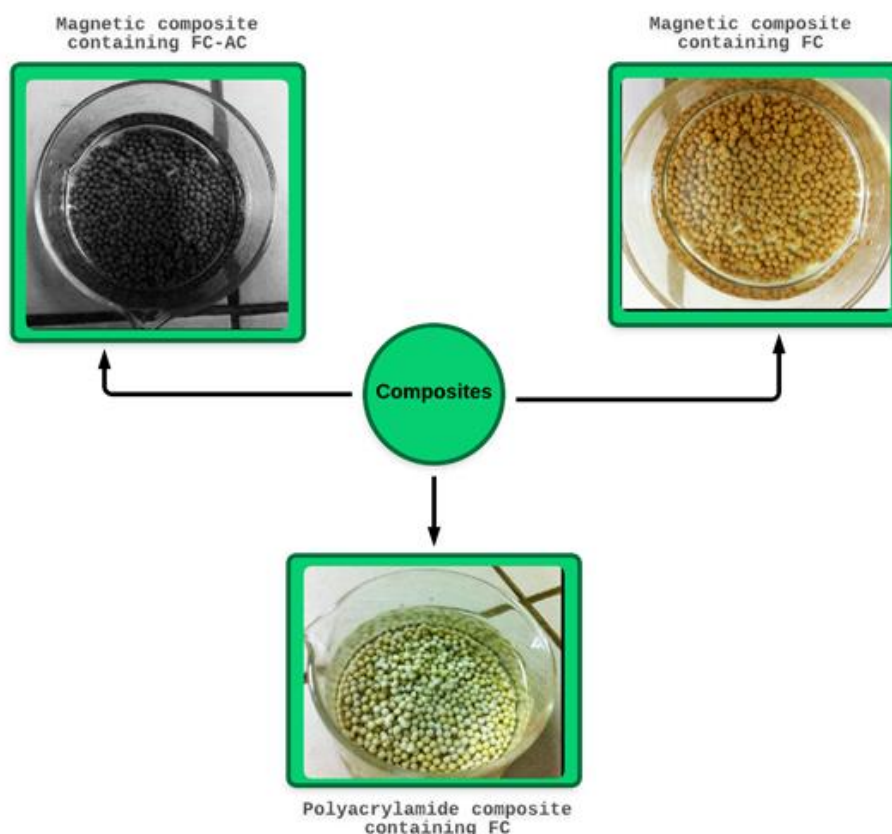


Figure 8: Synthesis pathway for magnetic hybrid composite and pictorial representation

3.4 Characterization of Adsorbents

The characteristic adsorptive capability of adsorbents is a function of their physiochemical properties including the nature of surface functional groups, surface area, availability and nature of pores present. In this thesis, all the adsorbents synthesized were characterized and results obtained are explained in detail. The surface functional groups of the adsorbents were assessed using Fourier transform infrared (Perkin-Elmer spectrophotometer FTIR-8700, USA). The point zero charges of the synthesized products were determined by drift method and detailed description could be found in our previous studies ([Oladipo et al., 2014](#) and [Oladipo and Gazi, 2014a](#)).

The pore structure of the as-prepared adsorbents were analyzed using N₂ adsorption technique, surface texture and morphology were examined using scanning electron microscope (SEM—JEOL/JSM-6300F) at an accelerating voltage of 20 kV. The Brunauer–Emmett–Teller surface analysis was performed to estimate the surface areas, total pore volumes and pore size distributions of the products. Boehm titrations were equally performed to quantify the basic and acidic surface groups on the materials and obtained results were observed to be consistent with other analyses data. Finally, the magnetic properties of the prepared materials were investigated by a vibrating sample magnetometer (VSM) at ambient temperature.

3.5 Experimental Adsorption Process

The batch studies were conducted in Erlenmeyer flasks (100 mL) containing the adsorbents and adsorbates under mechanical shaker at 150 – 200 rpm. Periodically, 5 mL samples were withdrawn from the reactor and the residual concentrations were analyzed by a UV–vis spectrophotometer (UV-Win 5.0, Beijing, T80+) at the maximum wavelengths of the adsorbate. The effects of sorption parameters (solution pH, dosage, initial adsorbate concentration, contact time, temperature and influence of co-existing ions) were investigated. The pH of the solution was adjusted with appropriate quantities of NaOH (0.1 M) and HCl (0.1 M).

The fixed-bed column studies were conducted in a glass column (30 cm; height and 2 cm; inner diameter) packed with wool at both ends in similar conditions with batch studies. The influence of bed heights and flow rates was examined until the effluent concentration transcended 95.5% of its influent concentration. The shapes of the breakthrough curve and breakthrough time are key characteristics for understanding dynamic operation and response of a sorption process in fixed-bed columns. The

breakthrough curves depict the sorption behavior of the adsorbates, and generally expressed in terms of influent concentration (C_i), outlet concentration (C_f), adsorbed adsorbate concentration (C_a), or normalized concentration (C_f/C_i) as a function of volume or time (Ahmad and Hameed, 2010). All sorption experiments were repeated three times to estimate the reliability of the data, and average results were reported.

3.6 Data Evaluation, Optimization, and Modeling

Data obtained from the batch and dynamic sorption studies were analyzed using the following equations (Oladipo et al., 2015; Tovar-Gomez et al., 2012; Zhao et al., 2014):

Single-component batch data analysis;

$$\text{Adsorption capacity } (q_e) = \frac{[M_i - M_f]}{W_{\text{ads}}} \times 100 \quad (1)$$

$$\text{Removal efficiency } (R_{\%}) = \frac{[M_i - M_f]}{M_i} \times 100 \quad (2)$$

Where M_i , M_f and W_{ads} are the initial adsorbate concentration, final concentration and weight of adsorbents respectively.

Binary-component batch data analysis;

Assuming there is no interaction and competition between the adsorbates. Hence, the total absorbance of a binary component system and concentration of each adsorbate can be expressed by Eqs. 3 and 4:

$$A_{\lambda_{\text{bin}}} = A_{\lambda_i} + A_{\lambda_j} \quad (3)$$

$$A_{\lambda_i, \text{bin}} = \varepsilon_{\lambda_i} C_i + \varepsilon_{\lambda_j} C_j + \dots \quad (4)$$

Fixed-bed column data analysis;

$$\text{Effluent volume } (V_{\text{eff}}) = Qt_{\text{tot}} \quad (5)$$

$$\text{Total amount of pollutant adsorbed } (q_{\text{tot}}) = \frac{Q}{10^3} \int_{t=0}^{t=\text{total}} C_a dt \quad (6)$$

$$\text{Maximum column capacity } (q_{\text{MC}}) = \frac{q_{\text{tot}}}{W_{\text{ads}}} \quad (7)$$

$$\text{Overall adsorption zone } (\Delta t) = -[t_b - t_e] \quad (8)$$

The constants in the binary equations are defined in the list of symbols, t_b and t_e represents the breakthrough time and exhaustion time respectively.

The experimental design and statistical importance of operating factors and their combinations were performed using SigmaXL (ver., 7.0, DiscoverSim, Canada). Central Composite Design (CCD) and Box–Behnken Design (BBD) were used to design the experimental runs in this study under extreme and narrow conditions respectively. The number of runs (N) needed for the development of CCD and BBD are defined respectively as $N = 2^j + 2j + C_0$ and $N = 2j(j-1) + C_0$, where C_0 is number of central axes and j represents number of factors (Gengec et al., 2013). The CCD and BBD generated quadratic equations for predicting the optimal adsorption conditions and can generally be expressed according to Eq. 9:

$$y = \alpha + \sum_{i=1}^j \alpha_i x_i + \sum_{i=1}^{j-1} \sum_{i=1}^j \alpha_{ij} x_i x_j + \sum_{i=1}^j \alpha_{ii} x_i^2 + \varepsilon \quad (9)$$

In Eq.9, the predicted response (y) correlated to the regression coefficients, quadratic coefficients, intercept and linear interactions. The coded factors of x_i , x_j represent the independent variables (adsorbate concentration, dosage, pH and contact time) at both narrow and extreme ranges as shown in Table 5. One of the main goals of this

research is to maximize pollutant removal efficiency and minimize operation cost; therefore, the operation cost was calculated. The composite, solution pH and effluent shaking were considered as the major cost items in the calculation of operating cost (₹m^{-3}) as expressed in Eq.10:

$$\text{Operating cost(OpC)} = xC_{\text{adsorbent}} + yC_{\text{shaking}} + zC_{\text{pH}} \quad (10)$$

Table 5: Experimental design for MBFC and levels of process factors

Variables	Units	Factors	Box–Behnken			Central Composite Design				
			Ranges and levels			Ranges and levels				
			-1	0	+1	- α	-1	0	+1	+ α
Adsorbent	mg	X ₁	20	50	100	20	40	80	160	200
Initial pH		X ₂	2.0	7.0	10	2.0	4.0	5.0	7.0	9.0
Conc.	mg/L	X ₃	50	100	200	50	100	300	400	500
Time	min	X ₂	90	180	360	30	60	120	240	480

3.7 Isotherm, Kinetic and Thermodynamic Studies

Adsorption isotherms give a good clarification of the interaction behavior between adsorbates and adsorbents (Acharya et al., 2009; Chieng et al., 2014). The commonly applied isotherms are Freundlich, Redlich–Peterson (R–P), Langmuir and Sips as listed in Table 6. In a multicomponent system of adsorbate solution, the interaction of adsorbate molecules may synergistically affect the sorption capacity of the adsorbents (Yan et al., 2014). Hence in this thesis, the sorption data were applied to a single component isotherm equations and the effect of multicomponent interaction on adsorbents sorption capacities were investigated via modified isotherm models in the batch system.

Table 6: Linear forms of isotherm equations and short description of the models

Isotherm models	Equations	Description
Freundlich	$\log q_e = \left[\frac{1}{n} \right] \log C_e + \log K_f$	The model provides multilayer sorption relationship between the adsorbents and the adsorbates.
Langmuir	$\frac{1}{q_e} = \frac{1}{q_m} + \frac{1}{C_e q_m K_L}$	Assumes that the maximum sorption relates to a saturated monolayer of adsorbates on adsorbent surfaces.
Sips	$\ln \left[\frac{q_e}{q_m - q_e} \right] = \left[\frac{1}{n} \right] \ln C_e + \ln K_s$	The combination of Freundlich and Langmuir isotherms for predicting heterogeneous sorption systems. It is necessary for low and high adsorbate concentrations that are restricted in other models.
R-P	$\ln \left[K_{RP} \frac{C_e}{q_e} - 1 \right] = \beta \ln C_e + \ln a_{RP}$	This is a three-parameter model that minimizes errors in earlier models

The contact time between adsorbent and adsorbate is quite significant for establishing the sorption mechanisms. Thus, four kinetic equations were utilized to analyze the experimental results as expressed in [Table 7](#).

Table 7: Kinetic equations and short description of the models

Kinetic models	Equations	Description
Pseudo—first—order	$q_t = q_e [1 - e^{-k_1 t}]$	Supports multilayer formation of adsorbates on adsorbent surfaces
Pseudo—second—order	$\frac{t}{q_t} = \frac{1}{k_2 q_e^2} + \frac{t}{q_e}$	Indicates the sorption processes proceed via chemisorptive pathway
Intraparticle diffusion	$q_t = k_{id} t^{0.5} + C$	Applied to predict rate-limiting steps associated with the sorption process.
Boyd	$B_t = -0.4977 - \ln \left[1 - \frac{q_t}{q_e} \right], D_c = \frac{B_t r^2}{\pi^2}$	Applied to predict the actual slow steps in sorption process.

The feasibility of the sorption process was also investigated via thermodynamic studies. Thus, the values of thermodynamic parameters (ΔS° , ΔH° , and ΔG°) were calculated for the adsorption of the adsorbates by the prepared adsorbents. These values are reported as a function of medium temperature and initial adsorbates concentration.

3.8 Desorption Experiments and Spent Adsorbents Reuse

The efficiency and performance of the saturated composite were investigated. This is done by rinsing certain quantity of the adsorbate-loaded adsorbents with NaOH (1.0 M), HCl (1.0 M) and ethanol mixture (v/v = 20/100, ethanol/water) in an Erlenmeyer

flasks. The flasks were agitated for 24 h and supernatant were withdrawn periodically. The concentration of the adsorbates was measured by UV–VIS at adsorbates specific wavelengths. Reuse of the desorbed adsorbent was conducted by rinsing the desorbed materials severally with distilled water and subjected to several cycles of adsorption-desorption tests. The performance of the adsorbents was recorded, and desorption mechanism explained.

Chapter 4

RESULTS AND DISCUSSION

4.1 Introduction

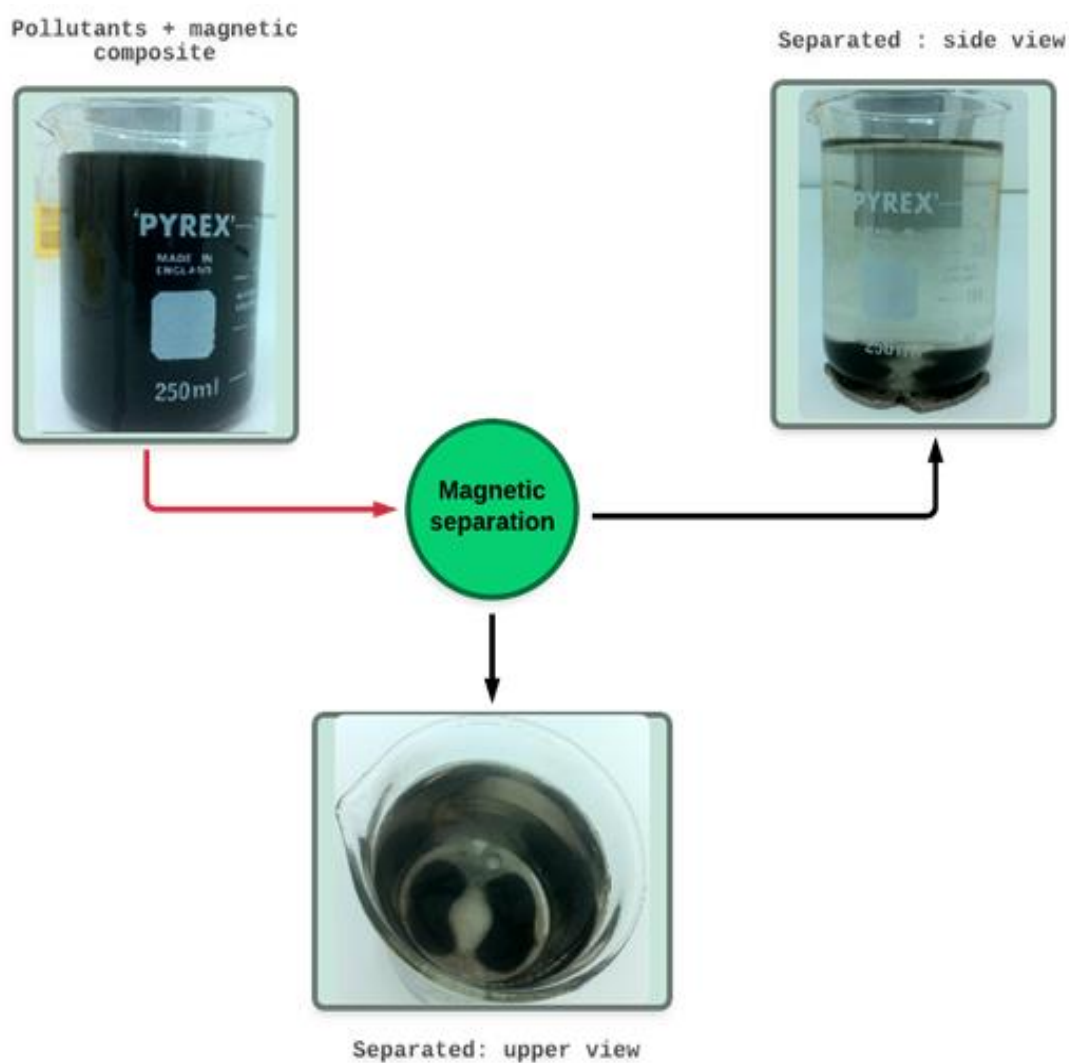
During the author's PhD program, following materials have been synthesized, utilized, and detailed preparation routes have been reported (Table 8). This thesis summarized the experimental data, synthesis procedures and characterization results already published and few unpublished data have been reported here. Some graphs and tables are reconstructed to capture this summary.

Table 8: Details of adsorbents synthesized and pollutants removed

Adsorbents	Pollutants Removed	Reference
Cellulose-based biocomposite hydrogel (EBH)	Reactive Blue 2 dye	Oladipo et al., 2014
Acid activated bentonite/alginate composite (AB-AC)	Crystal violet dye	Oladipo and Gazi, 2014a
Alginate-based composite (AB)	Nickel and Acid Red 25	Oladipo and Gazi, 2014b
Pomegranate based composite beads (PS-PVA)	Boron	Oladipo and Gazi, 2014c
<i>F. communis</i> biomass (FC)	Copper	Oladipo and Gazi, 2015a
Polyacrylamide-based activated carbon composite (PFCAC)	Copper and Direct Red 80 Nickel	Oladipo and Gazi, 2015a
Biomagnetic composite (MFC)	Acid red 25 dye	Oladipo and Gazi, 2015b
Nano-hydroxyapatite based composite	Nickel and Rhodamine B dye	Oladipo and Gazi, 2015c
Chitosan-based composite hydrogel (SAH)	Reactive blue and Erichrome black T dyes	Oladipo et al., 2015a
Bifunctional composite based on Cyprus coffee (MCC)	Phenol and Tetracycline	Oladipo et al., 2015b

4.2 Characterization

The physicochemical properties of the synthesized adsorbents are listed in [Table 9](#). The magnetic composites were dispersed in a flask containing the target pollutants, and external magnet (0.8 T) was applied below the flask to confirm the magnetic separability of the samples as shown in [Scheme 1](#).



Scheme 1: Illustration of magnetic separation of pollutants from simulated effluent

Table 9: Physicochemical properties of the synthesized adsorbents

Adsorbents Parameters	Values							
	FC	FC-AC	MFC	MFAC	PFC	PFCAC	MBAC	MBFC
pH _{pzc}	6.00	4.20	6.80	4.50	3.92	3.51	4.81	4.21
BET surface area (m ² /g)	445	1024.8	393	698.9	987	1156.3	678.9	897.8
Magnetization (emu/g)	—	—	69.32	56.98	—	—	78.98	98.67
Total pore volume (cc/g)	1.019	0.965	0.896	0.786	0.771	1.091	0.765	1.211
Average pore diameter (nm)	1.981	1.569	1.761	2.011	2.181	1.461	1.871	2.891
Functional groups (mmol/g)								
Phenolic	2.08	2.45	2.98	3.01	0.65	1.23	1.45	1.33
Lactonic	0.34	0.91	0.62	1.18	0.03	0.54	0.66	0.81
Carboxylic	0.91	1.01	1.45	0.56	—	0.03	0.04	0.02
Total acidic value	3.33	4.37	5.05	4.75	0.68	1.80	2.15	2.16
Amine content	—	—	—	—	1.34	1.08	1.21	1.41

The saturation magnetization of the synthesized copper ferrite nanoparticles (CuFe₂O₄) was determined as 68.3 emug⁻¹; hence magnetic properties were conferred to the composites via the integration of these nanoparticles. The SEM and FTIR analysis of the raw FC and the composites have been well described in the authors published paper referenced within. Characteristic peaks around 3500 – 3350 cm⁻¹ are attributed to the hydroxyl groups of lignocellulosic FC, the peaks around 1640.9 – 1650.7 cm⁻¹ confirmed the presence of –C=O groups and presence of CuFe₂O₄ particles was confirmed by band in the region of 569.1 to 620.11 cm⁻¹ (Oladipo and Gazi, 2015abc). Boehm titration was utilized to quantify the acidic

surface functional groups on the adsorbents. MBFC was utilized in the major part of the study due to its performance and magnetic separability.

4.3 Results of Optimization Studies and Statistical Analysis

The experimental design for adsorbates removals using MBFC and optimization of independent factors using BBD are shown in [Table 10–11](#).

Table 10: BBD experimental design for dye removal using MBFC

Run	Independent variables				Dye removal (%)			
	sorbent dosage (mg)	pH	Dye conc. (mg/L)	Time (min)	Dr80	Ar25	Cv	Rh
1	100	4	200	240	45.8	35.8	69.8	59.3
2	60	2	125	150	54.3	30.3	14.7	13.3
3	60	2	50	150	65.9	58.9	25.9	22.9
4	20	4	200	240	32.3	19.3	32.3	30.1
5	60	5	125	180	33.6	30.6	45.6	65.6
6	60	4	125	225	74.8	88.8	54.8	58.8
7	100	6	200	90	50.5	40.5	63.9	73.9
8	20	5	125	360	47.9	87.9	47.9	67.9
9	20	2	50	225	52.9	52.9	22.9	26.9
10	100	10	125	150	22.9	22.9	52.9	62.9
11	20	6	125	90	38.9	38.9	48.9	48.9
12	60	8	125	360	32.5	33.8	72.5	79.5
13	20	4	50	360	49.5	47.2	52.5	88.5
14	60	10	125	225	15.5	13.7	35.5	55.5
15	100	6	200	225	40.5	42.6	67.5	69.6
16	60	7	50	360	38.9	38.9	58.9	53.4
17	20	10	125	360	34.5	16.8	64.5	60.5
18	100	6	50	225	69.5	63.3	89.5	93.5
19	60	2	125	360	93.5	89.9	23.5	17.5
20	100	4	50	240	88.7	95.3	55.7	65.7
21	60	2	200	240	43.9	40.3	13.9	15.9
22	100	7	50	360	40.5	65.5	96.5	88.5
23	60	8	50	240	33.6	43.6	73.6	70.8
24	60	2	50	90	44.8	28.8	9.8	7.8
25	60	2	50	360	70.4	60.2	11.4	12.6
26	60	10	125	240	30.4	33.8	70.4	70.4
27	100	4	50	360	96.9	76.9	16.9	10.9

Table 11: BBD experimental design for heavy metal removal using MBFC

Run	Independent variables				Heavy metal removal (%)			
	sorbent dosage (mg)	pH	Metal conc. (mg/L)	Time (min)	Cu ²⁺	Ni ²⁺	Zn ²⁺	Mn ²⁺
1	100	7	50	360	92.8	85.3	79.3	69.3
2	20	7	50	360	54.3	56.3	50.7	53.7
3	20	8	50	360	88.9	50.9	85.7	87.9
4	20	5	50	360	55.3	38.3	32.3	40.8
5	20	2	50	360	13.3	10.6	9.6	5.6
6	20	10	50	360	64.8	69.8	64.3	88.8
7	100	6	50	90	50.5	40.5	63.9	73.9
8	20	5	125	360	47.9	87.9	47.9	67.9
9	20	2	50	225	12.9	14.9	22.9	16.9
10	100	10	125	150	72.5	69.9	66.6	62.9
11	20	6	125	90	68.5	65.1	58.2	53.3
12	60	8	125	360	72.5	73.8	72.5	79.5
13	20	4	50	360	29.5	27.2	22.5	28.5
14	60	10	125	225	75.5	63.7	65.5	55.5
15	100	6	200	225	40.5	42.6	67.5	69.6
16	60	7	50	360	58.9	48.9	58.9	53.4
17	20	10	125	360	84.5	86.8	69.5	60.5
18	100	6	50	225	69.5	68.3	79.5	73.5
19	60	2	125	360	13.5	19.9	23.5	17.5
20	100	4	50	240	38.7	35.3	35.3	35.7
21	60	2	200	240	13.9	10.3	13.9	15.9
22	100	7	200	360	42.5	65.5	66.5	68.5
23	100	7	200	90	30.6	33.3	43.2	40.8
24	60	2	50	90	10.1	8.8	9.8	7.8
25	60	2	50	360	10.9	10.2	11.4	12.6
26	60	10	125	240	30.4	33.8	70.4	70.4
27	100	4	50	360	6.9	10.2	16.9	10.9

The effects of four independent factors at three-level on dye/heavy metals removal from simulated wastewater were investigated using BBD approach. A total of 27 experimental runs were undertaken including 24 factorial, 3 axial and 3 replications at the center point. The analyzed experimental data were fitted to the second-order

polynomial equation, and various coefficients (regression, linear, quadratic and interaction) were obtained as shown in Eqs.11 and 12:

$$\begin{aligned} \text{Dye removal (\%)} = & 61.1 - 16.9X_1 - 8.15X_2 + 5.61X_3 + 2.73X_4 + 3.3X_1X_2 \\ & - 6.65X_1X_3 - 4.8X_1X_4 + 0.7X_2X_3 + 3.6X_2X_4 - 4.75X_3X_4 \\ & + 0.48X_1X_1 + 4.6X_2X_2 + 6.2X_3X_3 + 1.2X_4X_4 \end{aligned} \quad (11)$$

$$\begin{aligned} \text{Heavy metal removal (\%)} = & 74.1 - 23.5X_1 - 9.23X_2 - 4.93X_3 + 4.22X_4 + \\ & 5.2X_1X_2 - 5.95X_1X_3 + 5.02X_1X_4 + 1.5X_2X_3 + 2.9X_2X_4 - 4.33X_3X_4 \\ & + 0.92X_1X_1 + 3.99X_2X_2 + 8.1X_3X_3 + 1.8X_4X_4 \end{aligned} \quad (12)$$

The statistical significance of the models was assessed in the present work via analysis of variance (ANOVA) and presented in [Table 12](#).

Table 12: ANOVA from BBD for removal of heavy metal/dye using MBFC

Term	Sum of squares	DF	Mean square	F-value	P-value	Remarks
Model	13411	14	957.92	8.446	0.0003	Significant
X ₁ : pH	647.9	1	647.9	109.8	0.0000	
X ₂ : Conc. (mg/L)	598.9	1	598.9	0.56	0.0015	
X ₃ : Time (min)	387.9	1	387.9	0.87	0.3735	
X ₄ : Dosage (mg)	745.9	1	745.9	1.67	0.0391	
X ₁ X ₂	88.90	1	88.90	14.98	0.0065	
X ₁ X ₃	113.9	1	113.9	23.22	0.6023	
X ₁ X ₄	2,897.8	1	2,897.8	0.897	0.7550	
X ₂ X ₃	359.8	1	359.8	1.97	0.7206	
X ₂ X ₄	564.9	1	564.9	0.089	0.5743	
X ₃ X ₄	82.34	1	82.34	2.98	0.0425	
X ₁ X ₁	3.58	1	3.58	0.012	0.0006	
X ₂ X ₂	1.87	1	1.87	0.35	0.4345	
X ₃ X ₃	21.89	1	21.89	121.988	0.1520	
X ₄ X ₄	119.5	1	119.5	14.998	0.9802	
Lack-of-fit	1271.3	10	127.13	2.832	0.2891	Insignificant
Pure error	89.780	2	44.890			
Total (Model + Error)	14772	26	568.15			

The high coefficient of determination ($R^2 = 96.5 - 98.5\%$) and residuals of the ANOVA at 95% confidence level for the pollutants removals (Table 12) were utilized as criteria to validate the adequacy of the model. The high “*F-value*” (8.44) of the model that is greater than 4 is desirable. The “*P-value*” (0.0003) also indicates the statistical suitability of the model and implying that only 0.01% chance that the high *F-value* could occur by noise (Sadhukhan et al., 2013).

The “*P-value*” of the independent variables that are less than 0.050 shows that the model terms are statistically significant. In this research, insignificant lack-of-fit ($p = 0.289$) indicated that it is relatively inconsequential to the pure error, and hence, the experimental data were adequately represented by the model (Oladipo and Gazi, 2014a). As represented in Table 12, the *P-values* of pH (X_1), pollutant concentration (X_2), adsorbent dosage (X_4), interactive variables (X_1X_2 and X_3X_4) and quadratic solution pH (X_1X_1) are significant terms. Therefore, it is concluded that the operation factors played significant roles in the adsorption process according to the following order; pH > pollutant concentration > adsorbent dosage > contact time.

Three-dimensional response surfaces curves were developed based on the hierarchical quadratic equations and the optimum conditions and interactive effects of independent variables were obtained as shown (Fig. 9–10). In Fig.9, it is evidently obtained that solution pH strongly affects the pollutant removal efficiency because the adsorbent surface charge and adsorbate ionization changes with varying pH.

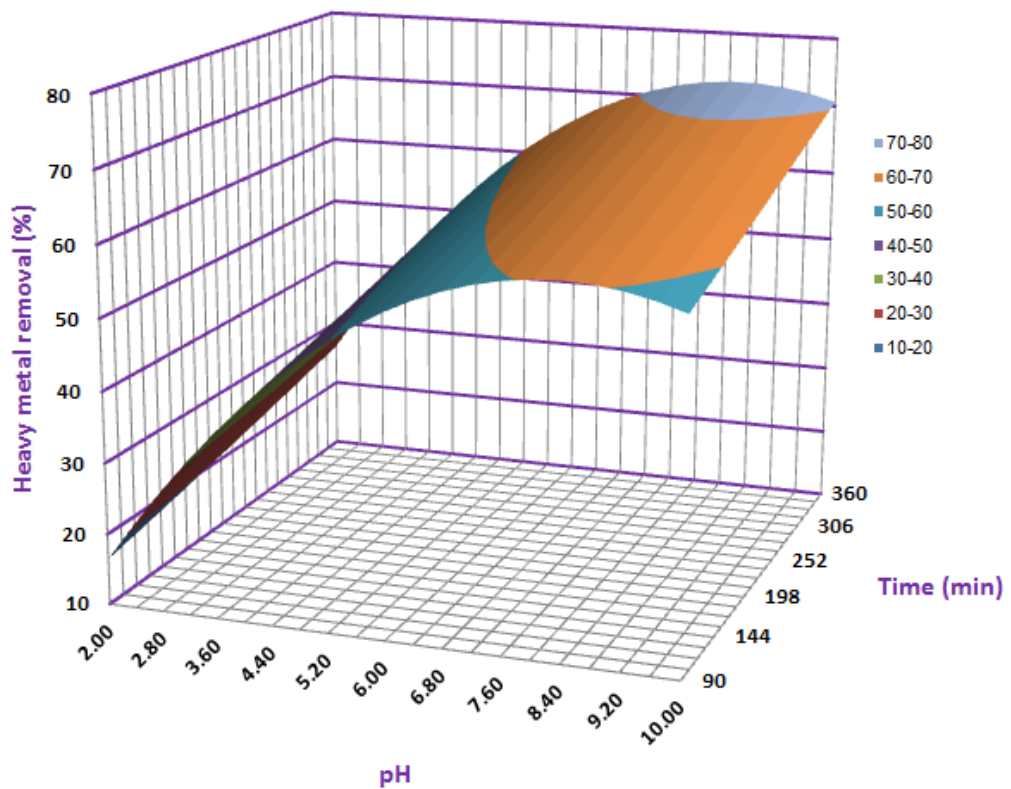
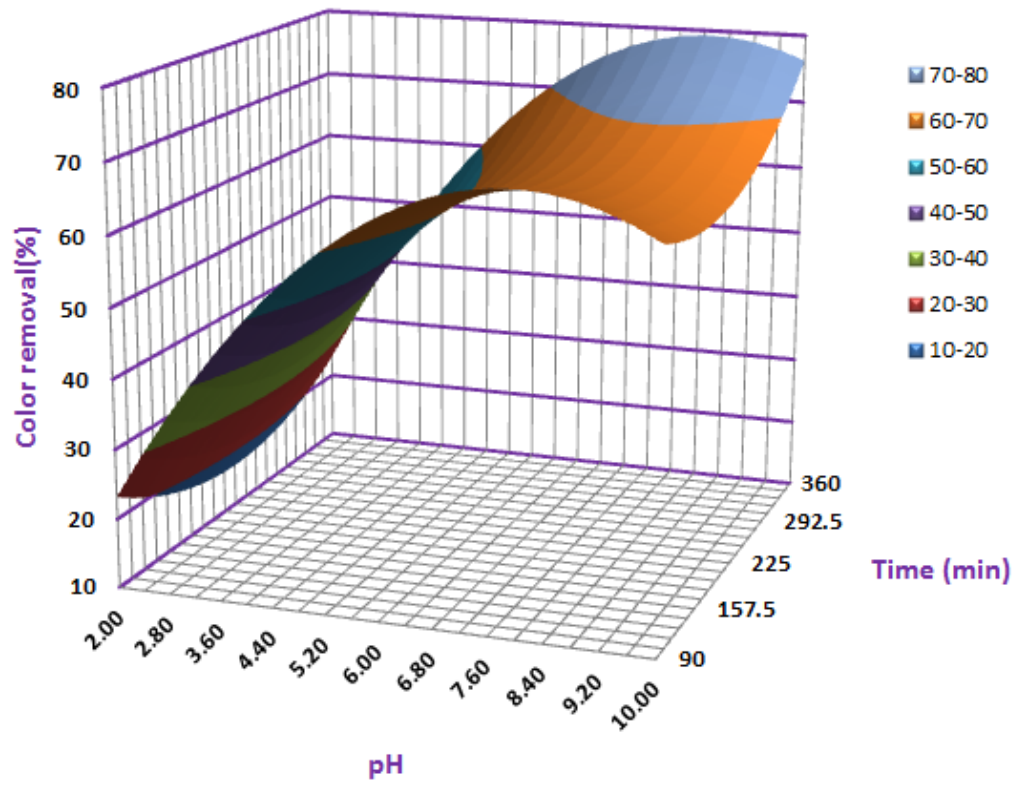


Figure 9: Response surface plots showing the interactive effects of pH and contact time

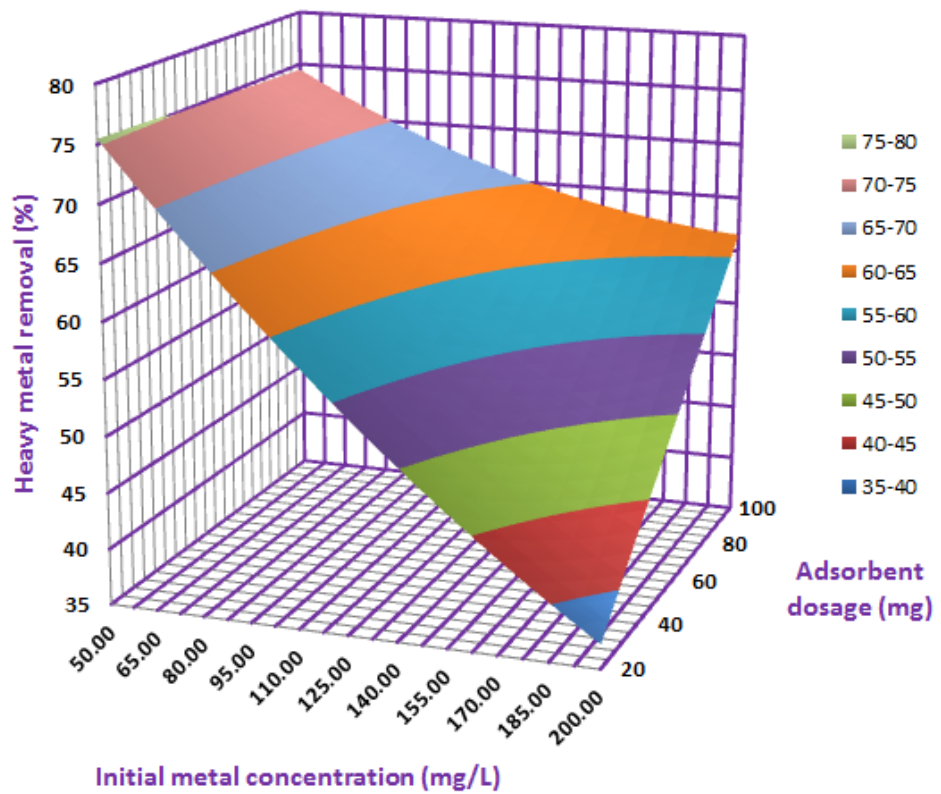
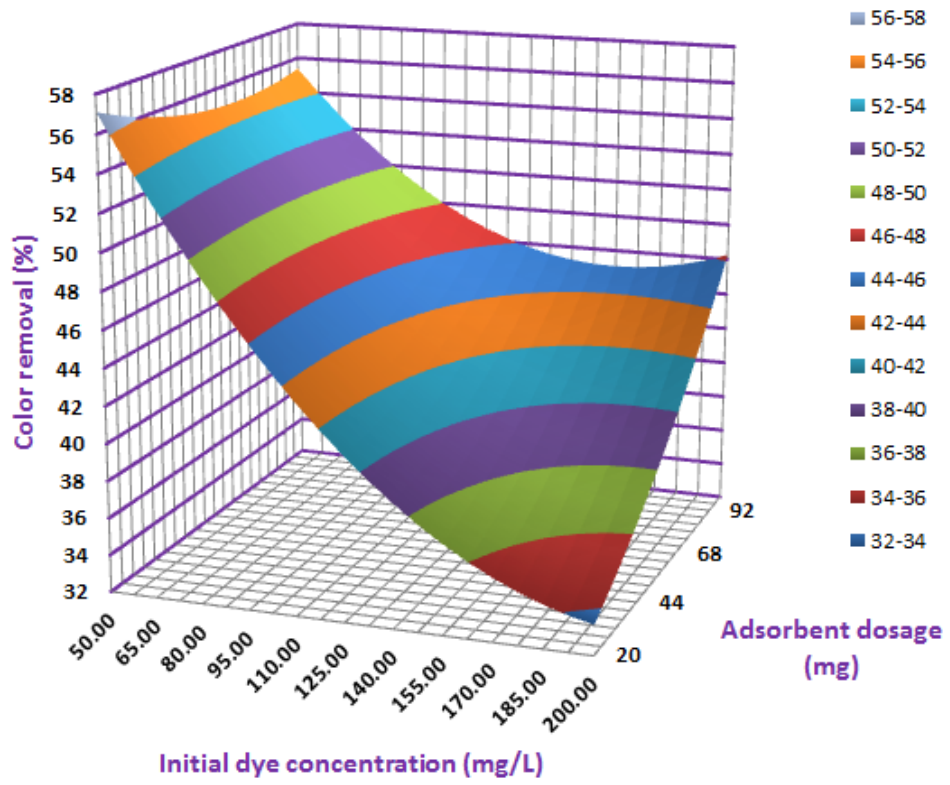


Figure 10: Response surface plots showing the effects of concentration and dosage

As expected, increasing pH of the solution contributes obviously to the removal efficiency as shown in Fig. 9; however, a decreasing trend in the removal efficiencies was attributed to electrostatic repulsion between the adsorbate anions and the adsorbent surfaces. Additionally, when all operating factors were held constant (runs 6 and 14) excluding the solution pH (Table 10), the removal efficiencies of the acidic dyes (Dr80 and Ar25) were noticed to decrease from 74.8–88.8% to 13.7–15.5% when the pH increased from 4 to 10 respectively. In contrast, the removal efficiencies of the investigated basic dyes (Cv and Rh) increased from 10.9–16.9% to 88.5–96.5% when the pH increases from 4 to 7 as indicated in runs 22 and 27.

Similar trends were observed for heavy metal removals as highlighted in Table 11. The 3D RSM plots confirmed that pH is a significant driving force to overcome mass transfer resistances of pollutants between the adsorbent surface and the solution. In acidic media, significant electrostatic attractions occurred between the protonated surface groups of the MBFC and the anionic dye molecules. Increases in solution pH above the MBFC point zero charge (PH_{pzc}) increased the quantity of negatively charged groups on the composite, thereby leading to decreases in removal efficiencies. Conversely, the basic dyes were less removed in acidic media due to repulsive forces between the cationic dye molecules and protonated MBFC surfaces (Chieng et al., 2014; Yan et al., 2014).

Variation in adsorbent dosages is another important driving force affecting removal efficiencies. In Table 11, when all factors were held constant excluding the composite dosage (runs 1 and 2), the heavy metal removal efficiencies increased from 50.7–56.3% to 69.3–92.8% when the MBFC dosage increased from 20 to 100

mg at pH 7. However, more noticeable changes were observed in the removal efficiencies (5.6–13.3%) for variation of composite dosages when the pH was 2 (run 5). This evidently supports the idea that pH is the most significant factor influencing sorption process of dyes and heavy metals from the simulated wastewater. The interactive effects of initial concentration of pollutants and composite dosages are presented in Fig.10. Increasing the initial pollutant concentration improves the interaction between the pollutants and the adsorbent, subsequently enhances the removed pollutant concentration (Bleiman and Mishael, 2010).

In this study, the removal efficiencies were noted to decrease with increases in initial pollutants concentration. This observation can be explained by the fact that, the surface area of the MBFC has specific sorption capacity, hence the decreasing pollutant removal efficiencies was likely due to insufficient sorption sites as the initial concentration increases (Oladipo et al., 2015ab). As indicated in Table 11, when all factors were held constant (runs 1 and 22) excluding the initial metal concentration, the heavy metal removal efficiencies decreased from 69.3–95.3% to 42.5–68.5% when the initial concentration of the investigated metals increased from 50 to 200 mg/L respectively. The effects of independent variables on removal efficiency and operating cost were assessed by using CCD approach. Data from preliminary experiments were analyzed by CCD and the experimental design shown in Table 13.

Table 13: Experimental design by CCD for heavy metal and dye removal using MBFC

Run	Independent variables				Pollutants Removal (%)				Costs (₹m ⁻³)		
	Dose (mg)	pH	Conc. (mg/L)	Time (min)	Cu ²⁺	Ni ²⁺	Zn ²⁺	Mn ²⁺	MBFC + pH	Shaker	OC
1	200	2	400	60	15.8	15.5	9.3	9.9	8.943	0.037	8.98
2	200	4	400	60	34.9	19.6	20.5	13.4	6.413	0.037	6.45
3	200	5	400	60	55.5	30.5	25.5	37.9	5.563	0.037	5.60
4	200	7	400	60	68.8	48.8	52.9	40.8	4.853	0.037	4.89
5	200	9	400	60	53.5	36.3	70.6	45.8	5.943	0.037	5.98
6	20	7	400	60	64.8	69.8	60.3	68.2	2.833	0.037	2.87
7	20	7	50	60	50.5	70.8	68.5	73.9	2.833	0.037	2.87
8	20	7	100	60	37.4	65.5	57.3	60.4	2.833	0.037	2.87
9	80	7	50	480	55.6	78.9	88.9	90.9	2.814	0.296	3.11
10	80	2	50	480	18.5	22.2	12.9	12.4	5.684	0.296	5.98
11	80	9	50	480	33.6	58.6	89.6	90.9	2.814	0.296	3.11
12	160	9	300	30	62.1	43.6	72.5	69.4	4.705	0.185	4.89
13	20	5	500	30	29.8	33.3	52.5	48.3	3.435	0.185	3.62
14	40	4	100	120	15.5	23.2	35.5	35.8	3.486	0.074	3.56
15	200	7	50	240	80.5	82.3	67.5	59.3	2.302	0.148	2.45
16	160	7	50	480	93.9	78.3	58.9	95.4	3.324	0.296	3.62
					Dr 80	Ar 25	Cv	Rh	MBFC + pH	Shaker	OC
17	200	4	50	480	89.5	93.6	24.3	20.9	3.813	0.297	4.11
18	200	4	400	60	53.5	49.9	20.5	19.3	3.943	0.037	3.98
19	200	5	400	60	48.5	45.8	25.3	25.9	4.313	0.037	4.35
20	200	7	400	60	23.5	20.8	63.5	65.3	3.193	0.037	3.23
21	200	9	400	60	42.5	65.5	66.5	68.5	5.083	0.037	5.12
22	20	7	400	60	30.6	33.3	43.2	40.4	4.943	0.037	4.98
23	20	7	50	60	44.8	68.8	39.8	45.3	4.943	0.037	4.98
24	20	7	100	60	70.4	60.2	61.1	62.8	4.943	0.037	4.98
25	80	7	50	480	30.4	33.8	74.3	79.8	4.154	0.296	4.45
26	80	2	50	480	37.4	65.5	17.3	10.9	5.044	0.296	5.34
27	80	9	50	480	55.6	78.9	88.9	90.9	4.814	0.296	5.11
28	160	9	300	30	18.5	22.2	82.7	85.5	6.045	0.185	6.23
29	20	5	500	30	33.6	58.6	89.6	90.9	2.935	0.185	3.12
30	40	4	100	120	62.1	43.6	71.8	59.4	3.466	0.074	3.54
31	160	4	50	480	92.8	33.3	68.6	48.8	4.182	0.148	4.33
32	160	7	50	240	15.5	23.2	85.3	95.8	6.702	0.148	6.85
33	200	7	50	480	80.5	82.3	90.5	94.3	3.684	0.296	3.98

Techno-economic analysis was performed and the electrical energy costs were obtained based on the TRNC retail electric unit cost in conjunction with Turkish Electricity Distribution Company tariffs (TEDAS, 2013).

Calculation of material and process costs:

As earlier stated within, the composite (MBFC), pH and shaker were only considered as major cost items during the adsorption process using Eq. 10.

Also;

- a. Energy consumption for shaking was calculated from the comparative unit cost of electricity from TRNC and TEDAS.
- b. Reagents costs were extracted from the manufacturer websites
- c. Raw *F.communis* was taken as zero cost
- d. Distilled water and eliminated water was factored as 1% in solution preparation

The conversion of raw *F.communis* (FC) into versatile hybrid magnetic composite (MBFC) (pre-treatment, ferrite process and crosslinking) was obtained as 0.59 ₺/kg MBFC, cost variation in the medium pH by NaOH and HCl ranges 0.169 – 0.811 ₺/kg HCl or NaOH and effluent shaking for 200 rpm was calculated based on unit charge as 0.037 ₺/h.

The economic analysis of the removal process of the investigated pollutants was realized via CCD approach in a narrow operation range. As shown in Table 13, increasing MBFC dosage led to increases in operation costs (OC), likewise the OC increased at lower pH but no significant effect was obtained on OC when the shaking time increased. One of the goals of optimizing the sorption process was to maximize the removal efficiency and minimize the operation costs. Considering these goals,

optimum removal efficiencies (93.9, 82.3, 89.6 and 90.9%) were obtained for Cu^{2+} , Ni^{2+} , Zn^{2+} and Mn^{2+} at operation costs (3.62, 2.45 and 3.11 $\text{₹}/\text{m}^3$) respectively. Similarly at optimum conditions, the average operation cost obtained from CCD for removal of the dye-pollutants is 4.98 $\text{₹}/\text{m}^3$, which is a relatively competitive price compared to other treatment technologies or adsorbent like charcoal ash reported by [Gengec et al., 2013](#). Hence, the optimum conditions for removal of the investigated heavy metals/dyes at low costs are runs 9, 11, 15–17 and 31–33 as indicated in [Table 13](#).

4.4 Effects of Independent Variables on Adsorbates Removal

It is obvious that various process variables including adsorbent dosage, temperature, operating time, pH, and adsorbate concentration influence the pollutant removal efficiencies. Therefore, the effects of these independent variables were assessed in single and binary component systems.

4.4.1 Batch Studies

The adsorption data obtained from the sorption process in batch mode is helpful in providing information relating to the effectiveness of the pollutant-adsorbent system. However, such data are practically not applicable to industrial treatment system such as column operations. Hence, in this study both batch and column studies were performed and data obtained were observed to be logically consistent.

Effect of Solution pH in Single Component System

The pH does not only influence the solution chemistry, but also causes the adsorbents surface functional groups to either deprotonate or protonate, hence affecting the adsorption efficacy with various adsorbates ([Chathuranga et al., 2013](#)).

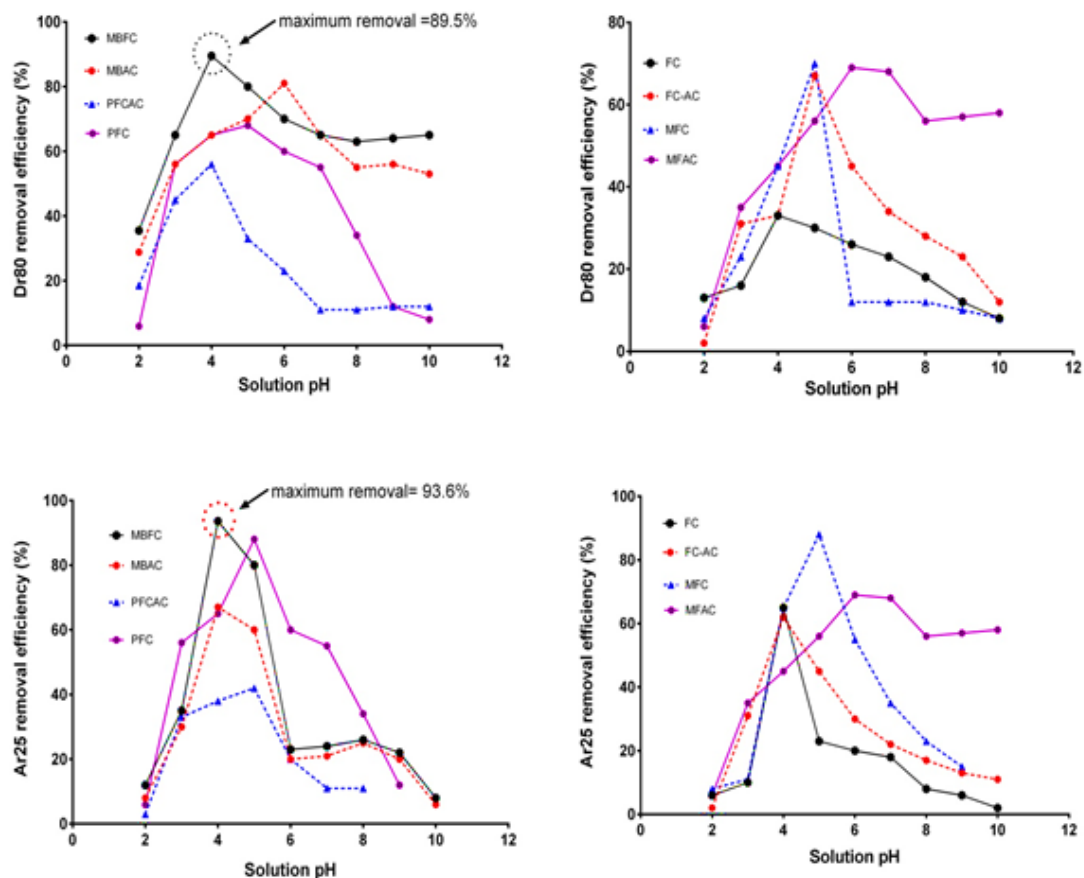


Figure 11: Effect of pH for acidic and cationic dyes removal by various adsorbents

In this research, the effect of solution pH on the removal of each pollutant was varied from 2.0 to 10.0 at 50 mgL^{-1} initial pollutant concentration. The pH point zero charges (pH_{pzc}) for each adsorbent is listed in Table 9. For the single component adsorption system of the dyes (Fig. 11), it is evident that the percent removal of Dr80 and Ar25 increases with increase in solution pH from 2 to 6.0, but no obvious adsorption noticed after pH 6.0. When the solution pH was higher than the pH_{pzc} , decreasing trends were noticed for the acidic dyes. On the other hand, lower sorption of cationic dyes (Cv and Rh) was observed at acidic pH which may be ascribed to the electrostatic repulsion between the positively charged dye molecules, the protonated adsorbents surfaces and excess H_3O^+ ions in the solution (Fig.12).

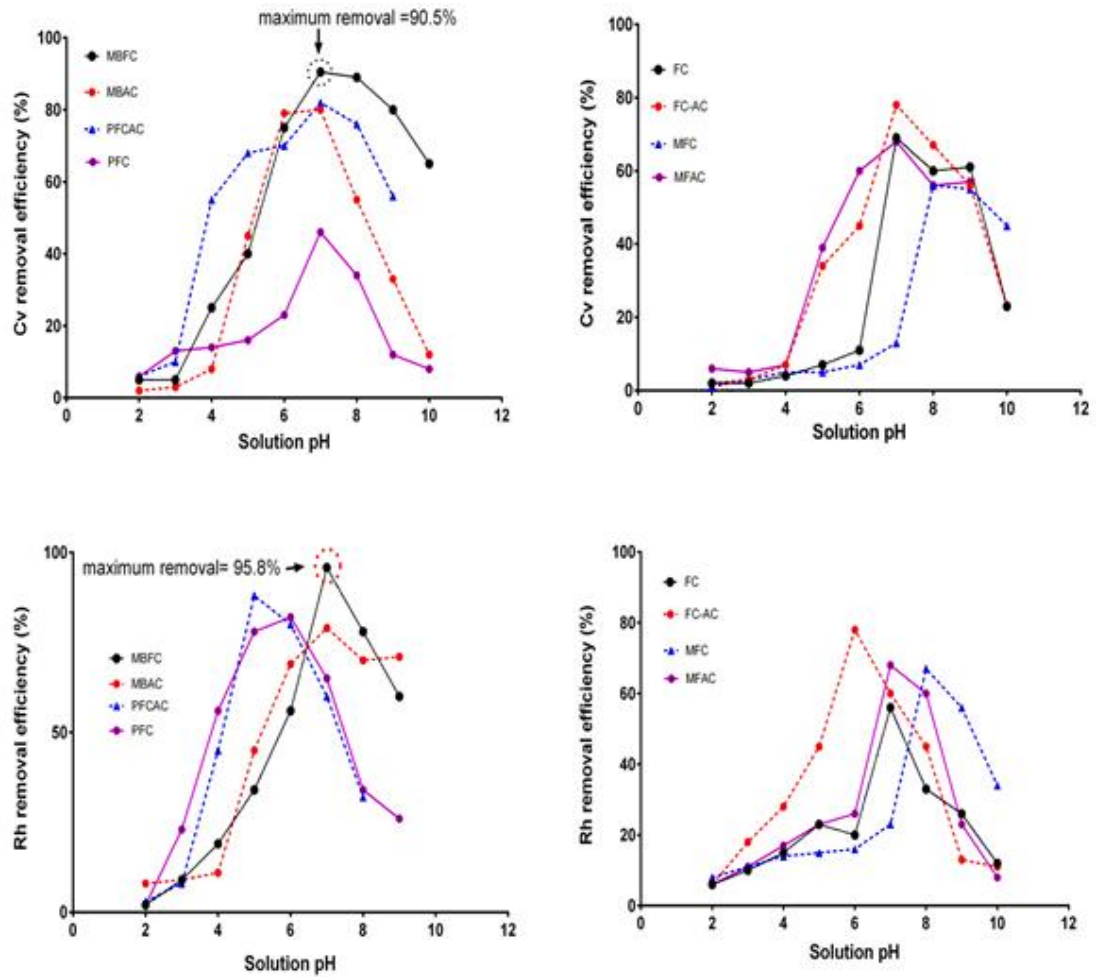


Figure 12: Effect of solution pH on the removal of cationic dyes by various adsorbents

Similar trends are noticed during the removal of heavy metal, and the percentage of heavy metal removed increases at $\text{pH} > 6.0$ which is likely due to a reduction in H_3O^+ concentration and deprotonation of the adsorbents surface groups. The experimental data were fitted into the surface complexation model (SCM) so as to enhance the understanding of the heavy metals removal mechanism. The SCM assumes that adsorbent surface functional groups can be grouped into three based on the protonation reactions (neutral: YOH , negative YO^- , and positive: YOH_2^+) and metal adsorption basically takes place through complexation with surface groups in the form of YOM^+ (viz.; YONi^+ or YOCu^+).

In this part of the thesis, the pH effect on heavy metal ions was assessed from pH 2.0 to 14 so as to understand the metal speciation and fractions adsorbed. Y and M⁺ are used in SCM modeling and represent the adsorbent and metal ions respectively. As shown in Fig. 13a, the YO₂Cu⁺ fraction adsorbed onto FC increased with increasing medium pH until it reached a maximum at pH 7.0, and then converted into Cu(OH)₂ after being released from the FC surface. The fraction of YO₂Cu⁺ removed reached 70% at pH 6.3 during the increased stage. However, the fraction of YO₂Cu⁺ removed at the decreasing stage was less than 20% when the solution pH 10. A similar trend was noticed when MBFC was used, however, when the solution pH increased to more than 7.5, the YO₂Cu⁺ fraction removed was higher than 50.5%. This result of MBFC as compared with FC suggested that MBFC could remove more pollutant even at extreme pH during copper adsorption. The Zn²⁺ and Ni²⁺ show similar trends like Cu²⁺.

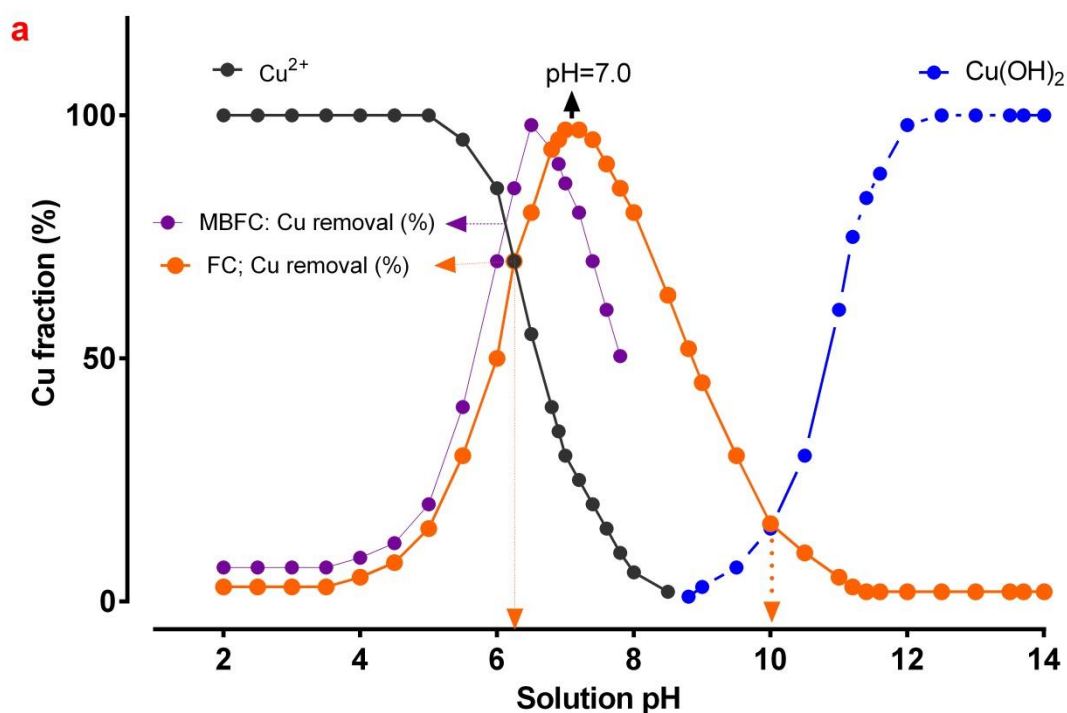


Figure 13: (a) Simulations of copper ion speciation and sorption by adsorbents

By contrast (Fig.13b), the removal of Mn^{2+} by FC and MBFC was slower than that of other investigated heavy metal ions. Only 45% of $YOMn^+$ was removed at pH 7.0 for FC and 52% for MBFC pH 6.7, but maximum adsorption was attained at pH 8.0 for FC and pH 7.0 for MBFC. The data obtained suggest that the removal of Mn^{2+} by FC occurred at a higher pH when compared with the other metal ions. Additionally, 1.5 – 2% of $YOMn^+$ on FC and MBFC was released into the medium and converted into $Mn(OH)_2$ at pH 9.0. This may be as a result of Mn^{2+} hydrolysis, and similar observation has been reported by Zhang et al., 2015. In conclusion, SCM confirmed that the metals appear predominantly as M^{2+} species at pH < 6.5, M^{2+} adsorption edge begins at pH 2 until it reaches maximum at pH 7–8 and, thereafter their concentration decreases to form various metal hydroxyl species ($Y(OH)_2$ predominately). Also, the removal sequence of these metals was $Cu > Ni > Zn > Mn$ which may be a combination of surface complexation and electrostatic interactions.

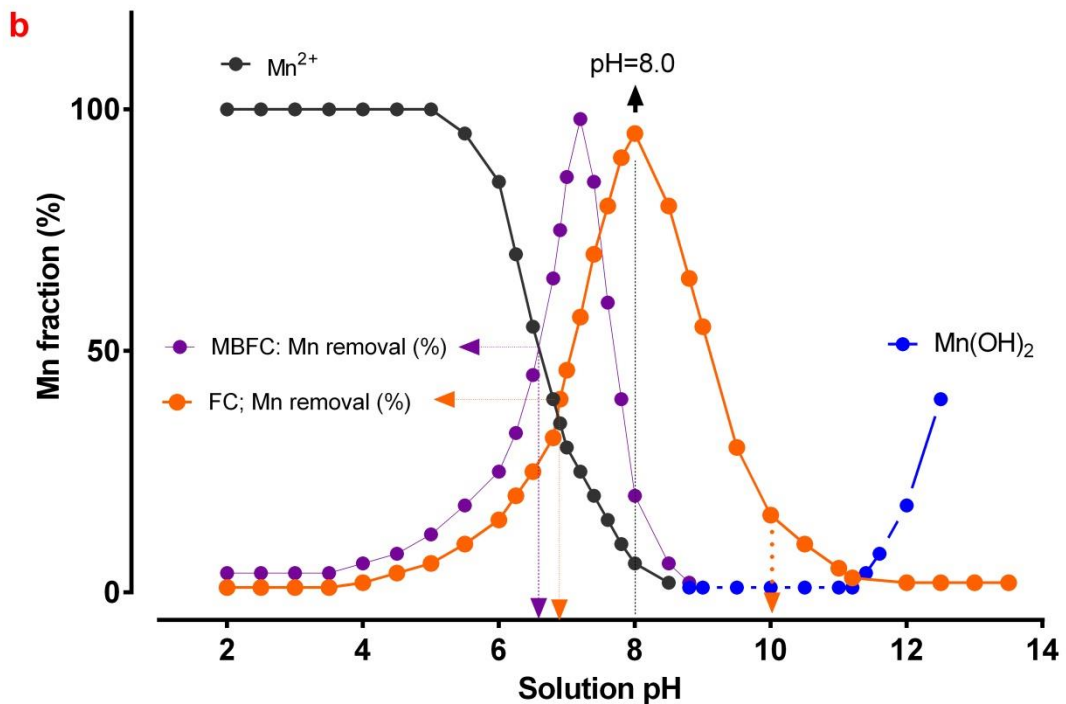


Fig. 13: (b) Simulation of manganese ion speciation and sorption by adsorbents

Effect of Adsorbent Dosages in Single Component Systems

Investigation on the effect of variation in adsorbent dosages reveals that there is a rapid increase in percentage removal of the pollutants at the initial stage, and then a moderate increase followed by constant pollutant removal was observed. It can be seen in Fig. 14a at pH 7.0 that initially the copper percentage removal increases sharply from 17.5 to 93.9% with the increase in MBFC dosage from 20 to 160 mg. However, beyond 160 mg, no significant removal was observed.

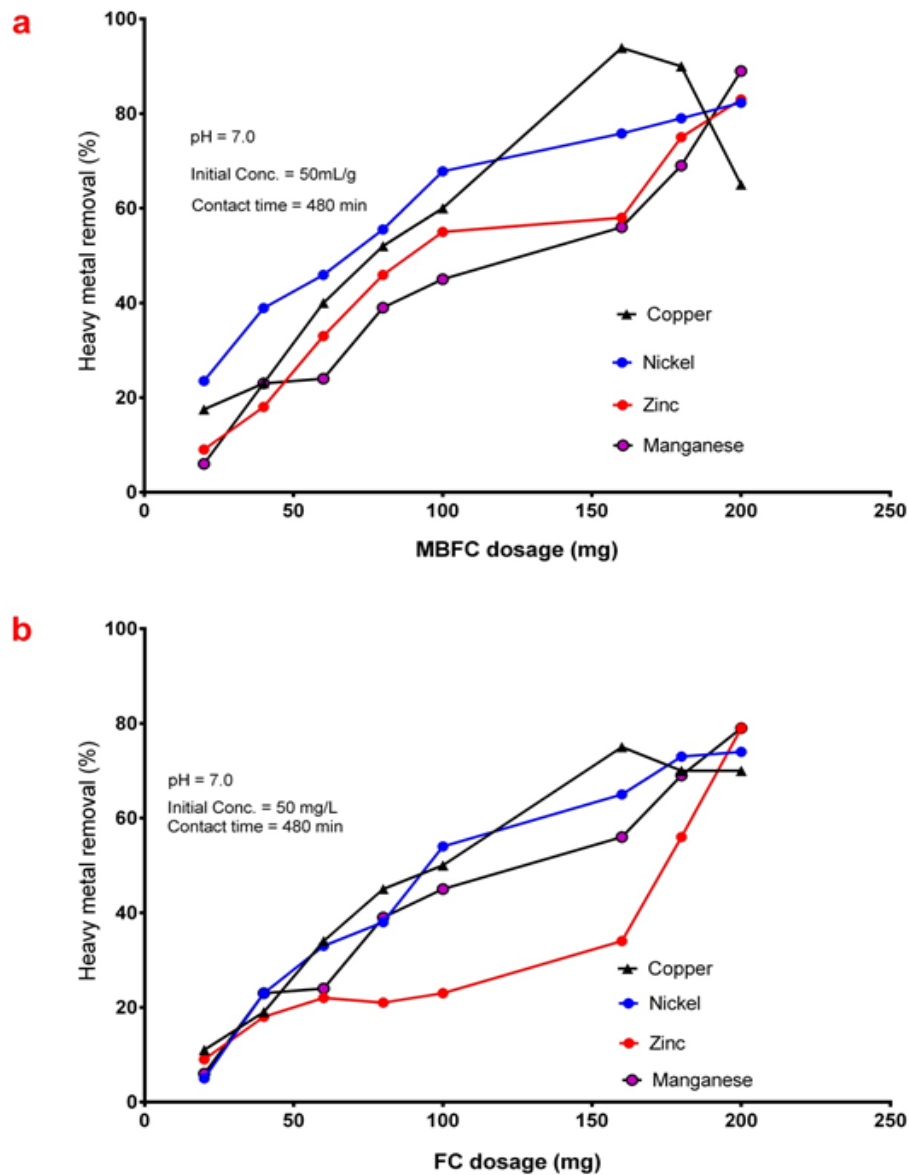


Figure 14: Effect of (a) MBFC and (b) FC dosage on heavy metal removal

The FC was observed to shrink after the experiment and the copper removal percentage was lower compared with MBFC (Fig.14b). The higher removal percentage obtained when MBFC was used is expected because it contains more sorption sites and mechanically stronger as compared with FC (Oladipo and Gazi, 2015a).

As the adsorbent dose increases the number of available sorption sites increases as well leading to more sorption. A moderate increase in the percentage removal observed beyond 160 mg may be due to saturated sorption sites (Imamoglu, 2013). For a nickel, the removal percentage increases from 23.5 to 82.3% when the MBFC dosage increases from 20 to 200 mg. As indicated in Fig. 14, similar trends were observed in the removal percentage of all investigated pollutants. Data obtained complied with CCD results. Hence, the use of MBFC is justified for both performance and economical purposes.

Effect of Ionic Strength in Single Component Systems

The effect of ionic strength on MBFC removal efficiency was investigated. Fig. 15 shows the adsorption of heavy metals and dyes on MBFC in the presence of 0.01M KCl, LiCl and NaCl respectively, as a function of pH values. As shown, the adsorption of the metal ions by MBFC was weakly affected by the cations in the reactor. Evidently in Fig. 15, the adsorption of metal ions within the same pH values follows this sequence; $K^+ < Na^+ \approx Li^+$, specifying that the cations can modify the surface character of the MBFC and hence can affect the sorption process of the metal ions. The order of metal uptake was observed to be highest in the presence of lithium

and can be attributed to the cations radii of hydration Li^+ : $3.4 \text{ \AA} > \text{Na}^+$: $2.76 \approx \text{K}^+$
 $=2.32$ (Xu et al., 2008).

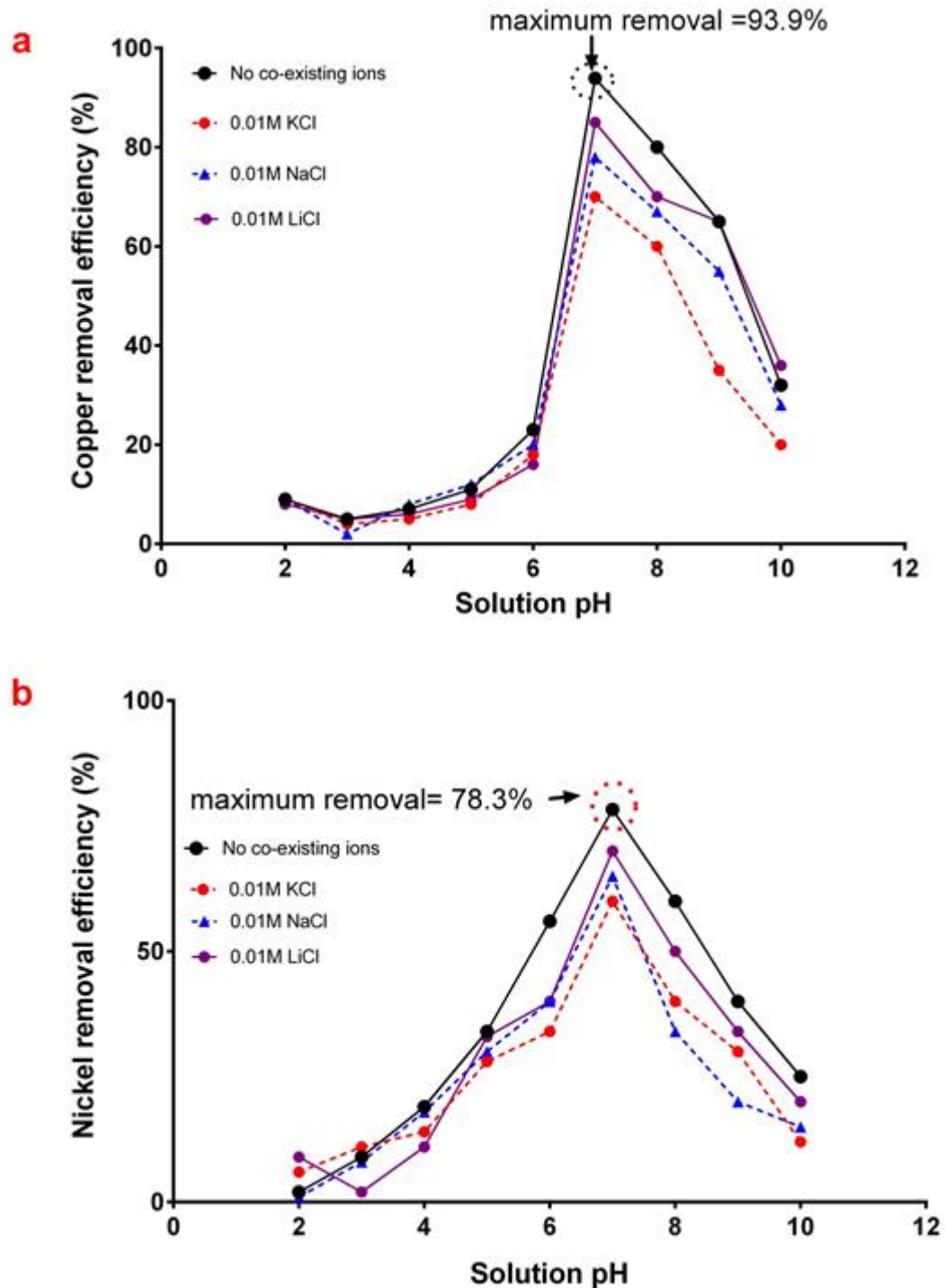


Figure 15: Variation in adsorption of (a) Cu and (b) Ni by MBFC as a function of pH and foreign cations

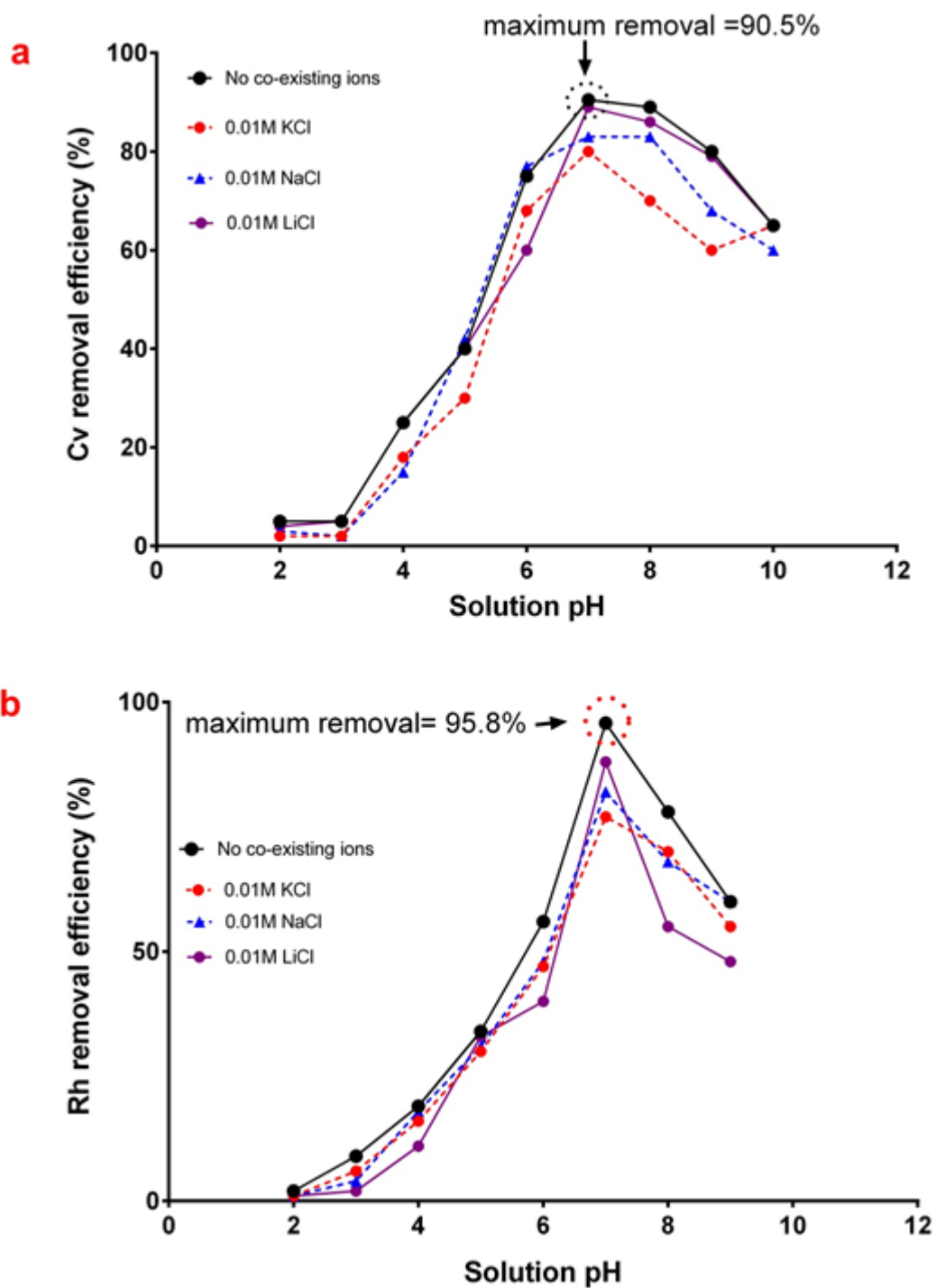


Figure 16: Variation in adsorption of (a) Cv and (b) Rh cationic dyes by MBFC as a function of pH and foreign cations

The lower adsorption obtained in the presence of co-existing ions is ascribed to electrostatic competition between the cations and the metal ions at the MBFC surfaces. It is clear that the suppression of the metal uptake in the presence of the

monovalent cations was low at $\text{pH} < 6.5$. However, at $\text{pH} 7\text{--}10$, the influence of the co-existing cations was substantial. On the other hand, the co-existing cations have no obvious effect on Dr80 and Ar25 adsorption, and their influence was also weak in the presence of cationic dyes (Fig. 16). It can be concluded that outer-sphere complexation and other interactions are responsible for the pollutant adsorption since the removal efficiencies decrease with increasing ionic strength (Liu et al., 2009).

4.4.2 Fixed-bed Studies

To confirm the suitability of the prepared bio-based composite, MBFC was applied in the fixed-bed system, and the effects of bed depth and flow rates were assessed.

Effect of Bed Depth on Pollutant Removal

The breakthrough curves at various bed depths for dynamic adsorption of acidic dyes by MBFC are shown in Fig. 17. It can be seen that as the bed depth increased, Dr80 and Ar25 ions had more contact with the adsorbent, resulting to increased removal efficiency of the pollutants. Hence, the higher bed column led to a decrease on the adsorbates concentration in the simulated effluent. The breakthrough time for 50 mgL^{-1} initial Dr80 concentration at $C_f/C_i = 0.5$ was observed to be 40, 45 and 80 min when the bed depth was 2, 4 and 8 cm, respectively. We can see that the slope of the breakthrough curves decreased with increases in bed column which led to a broadened influent mass transfer zone.

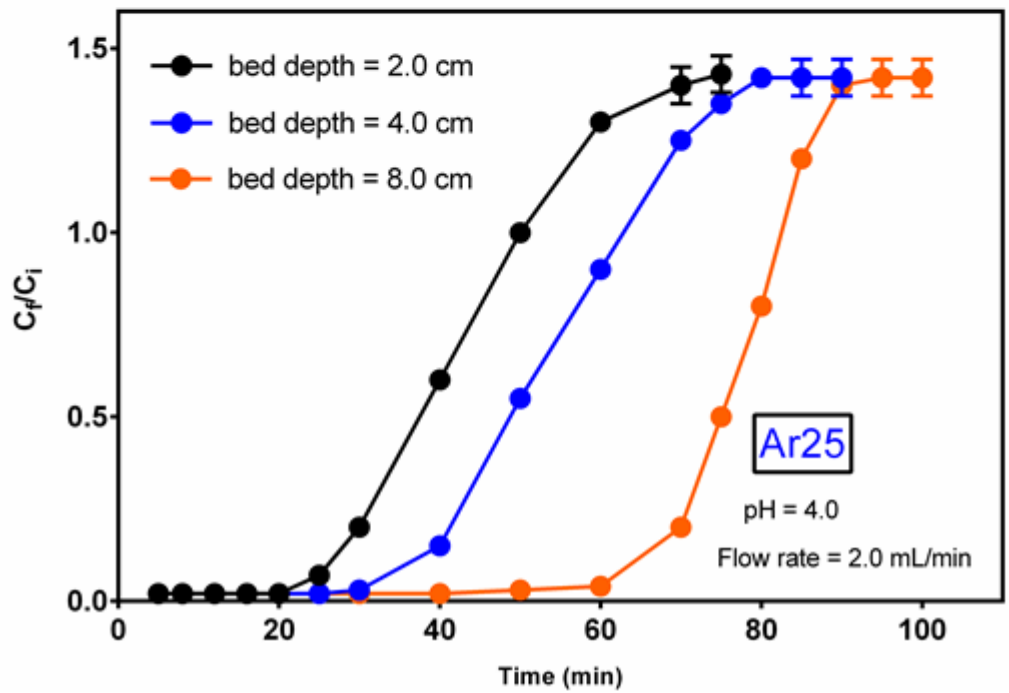
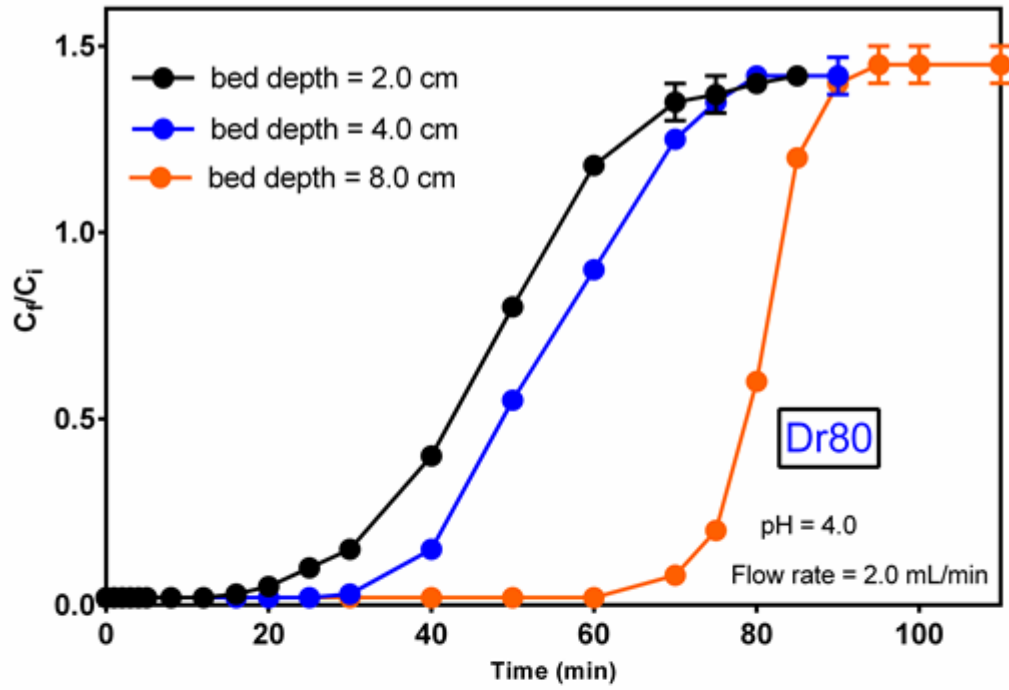


Figure 17: Effect of bed depths on acidic dyes adsorption by MBFC

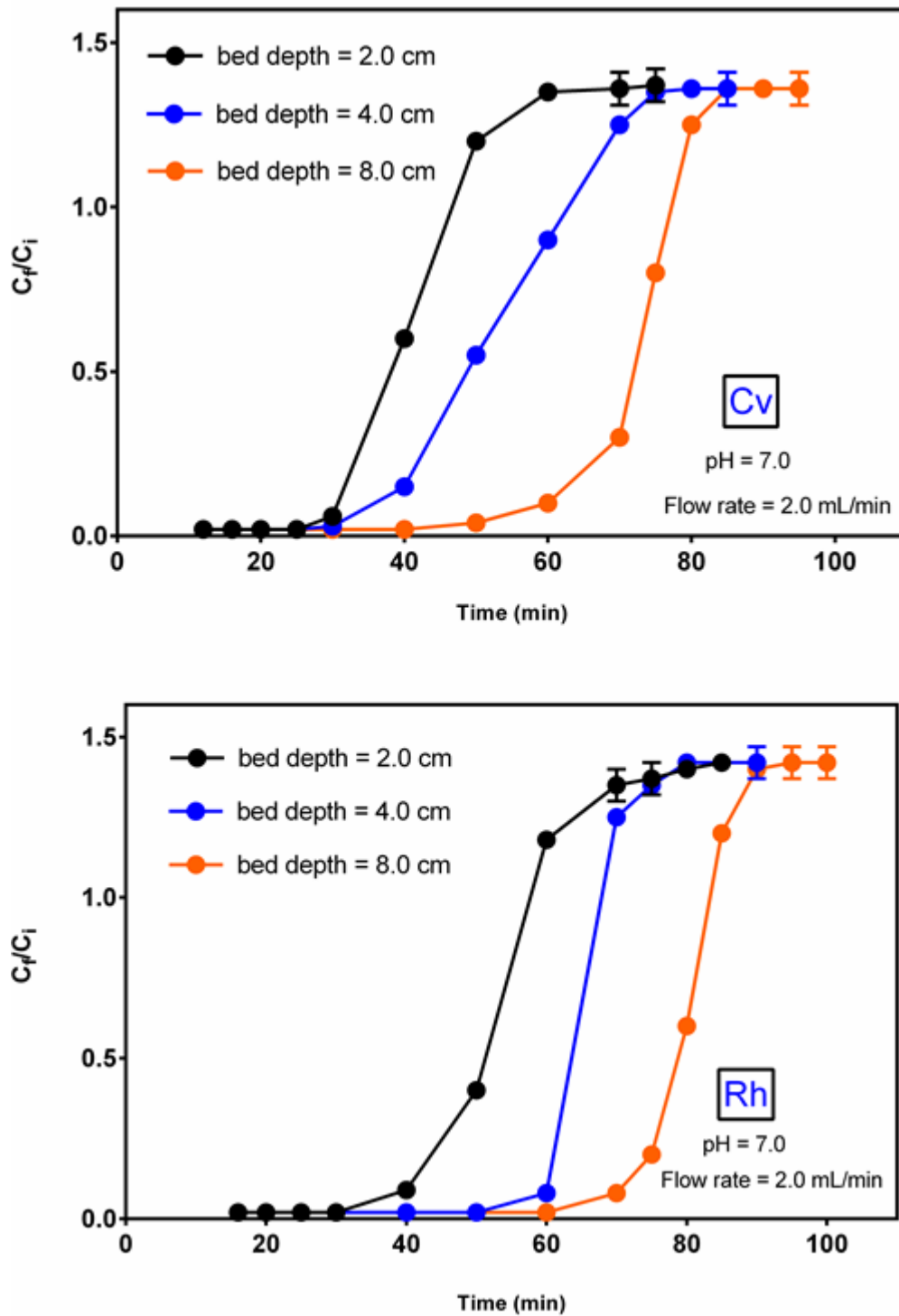


Figure 18: Influence of bed depth on the removal of cationic dyes by MBFC

The higher removal efficiency obtained at higher bed depth is due to increases in the surface area and presence of more sorption sites for binding Dr80 molecules (Zhao et al., 2014). Similarly at pH 4.0 and 2.0 mLmin⁻¹ flow rate, both the breakthrough

time and the removal efficiency for Ar25 increases with increases in bed depth. Therefore, it is concluded that the lower bed column results in an increase in the Ar25 concentration in the reaction mixture at the same operating time. The breakthrough time for 50 mgL^{-1} initial Ar25 concentration at $C_f/C_i = 0.5$ was obtained to be 31, 50 and 78 min when the bed depth was 2, 4 and 8 cm, respectively. Similar trends were observed when the removal of the cationic dyes was assessed in the fixed-bed system at pH 7.0 and constant flow rate. Fig. 18 shows the influence of bed depth on Cv and Rh removal by MBFC. The influence of bed depth on heavy metals removal was assessed and data obtained are indicated in Fig. 19–21.

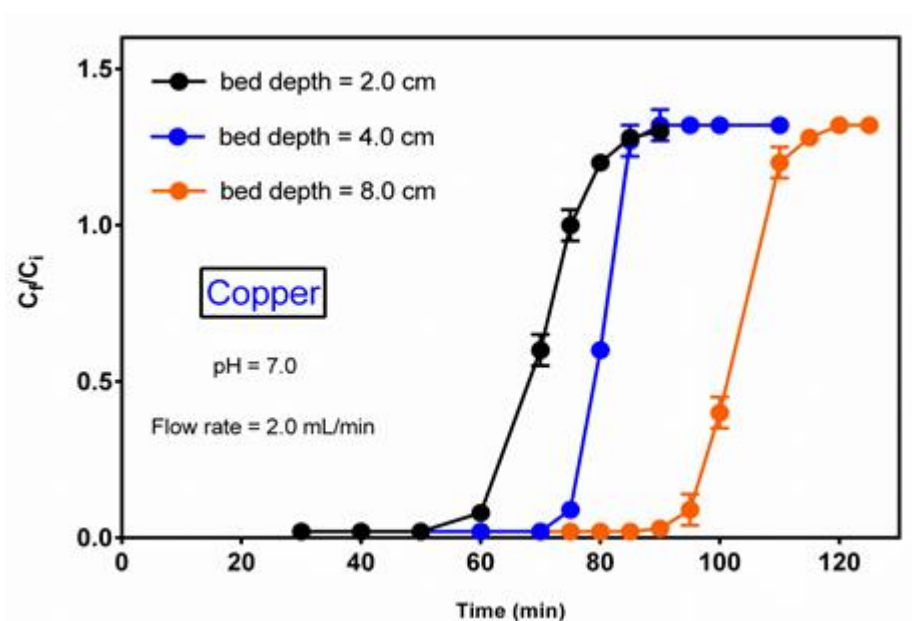


Figure 19: Effect of bed depth on copper removal by MBFC

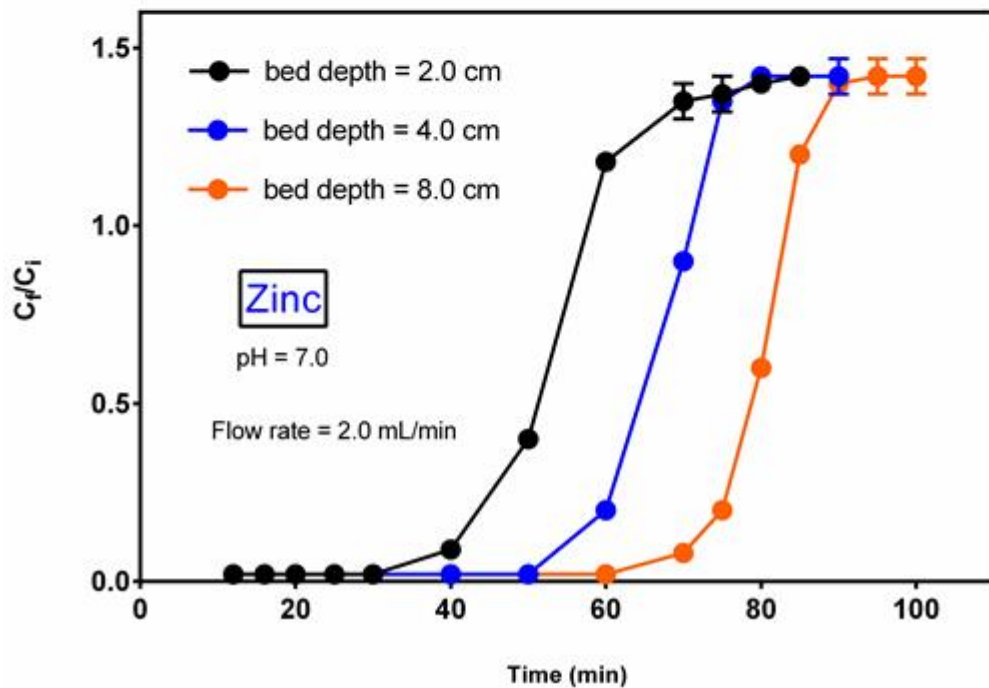
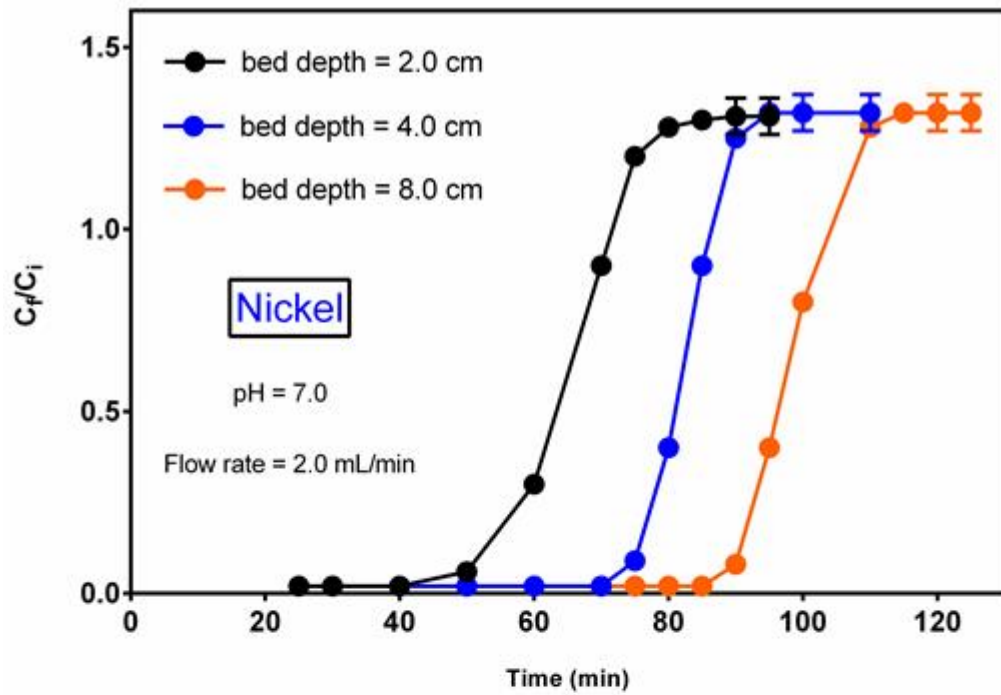


Figure 20: Effect of bed depth on nickel and zinc removal by MBFC

It can be seen that in all cases breakthrough times increased with increases in bed depth. For instance, the breakthrough time for 50 mgL^{-1} initial copper concentration at $C_t/C_i = 0.5$ was obtained to be 62, 78 and 100 min when the bed depth was 2, 4

and 8 cm, respectively. Similarly, the exhaustion concentration increased with bed depth resulting in higher removal percentage. As earlier noticed in the batch experiments, the removal of Mn^{2+} tend to be slower as compared to other metal ions. A similar observation is noticed in the fixed-bed removal of Mn^{2+} using MBFC. As compared with copper removal at $C_f/C_i = 0.5$, Mn^{2+} breakthrough times are 24, 40 and 60 min when the bed depth was 2, 4 and 8 cm, respectively. However, the Mn^{2+} uptake capacity is in the same range with Cu^{2+} .

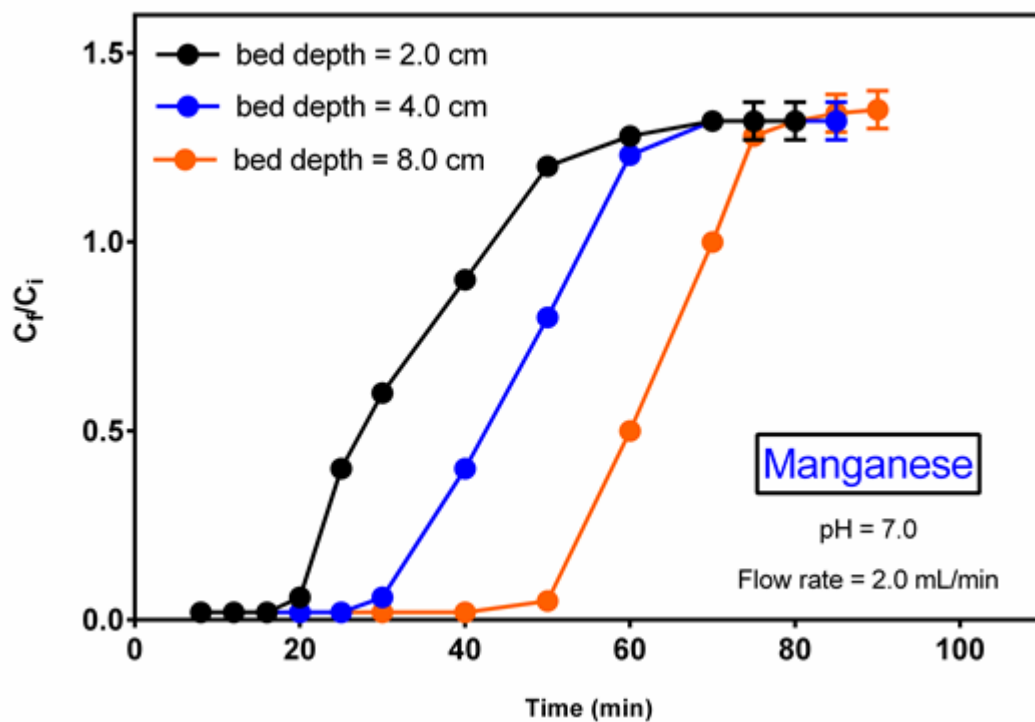


Figure 21: Effect of bed depth on manganese removal in bed column of MBFC

Effect of Flow Rates on Pollutant Removal

The effect of variation in flow rates ($2.0 - 10.0 \text{ mLmin}^{-1}$) at constant bed depth of 8.0 cm and 50 mgL^{-1} pollutant concentration was examined. The breakthrough curves at different flow rates for the investigated pollutants are shown in Fig. 22. It is noticed that the breakthrough curves became flatter with decreases in flow rate.

Hence, it can be concluded that breakthrough time decreased at a same normalized concentration (C_f/C_i) when the flow rate increased. [Zhao et al., 2014](#) reported similar trend when Congo red was adsorbed in the column of surfactant modified wheat straw. They attributed the decreasing breakthrough time to the insufficient residence time of Congo red molecules in the column when the flow rate increases.

In all cases, the breakthrough was delayed at a lower flow rate. Breakthrough time of the MFBC reaching saturation decreased obviously with an increased in the flow rate. As shown in [Fig. 22](#) at a low flow rates, the influent Dr80 and Ar25 had more contact time with MBFC that led to the higher removal of the dye molecules in the fixed-bed column. Hence, the variation in the uptake capacity and the slope of the breakthrough curve can be explained using mass transfer concept. As reported by [Oladipo and Gazi, 2014ab](#), the rate of mass transfer increases at higher flow rate, meaning the quantity of adsorbate adsorbed onto MBFC unit bed height increased resulting in faster saturation of beds at higher flow rate. Due to the insufficient residence time of the adsorbate in the column before equilibrium and less interaction with the MBFC sorption sites, lower uptakes were achieved. Results obtained are consistent with those reported in the literature ([Ahmad and Hameed, 2010](#); [Zhao et al., 2014](#)).

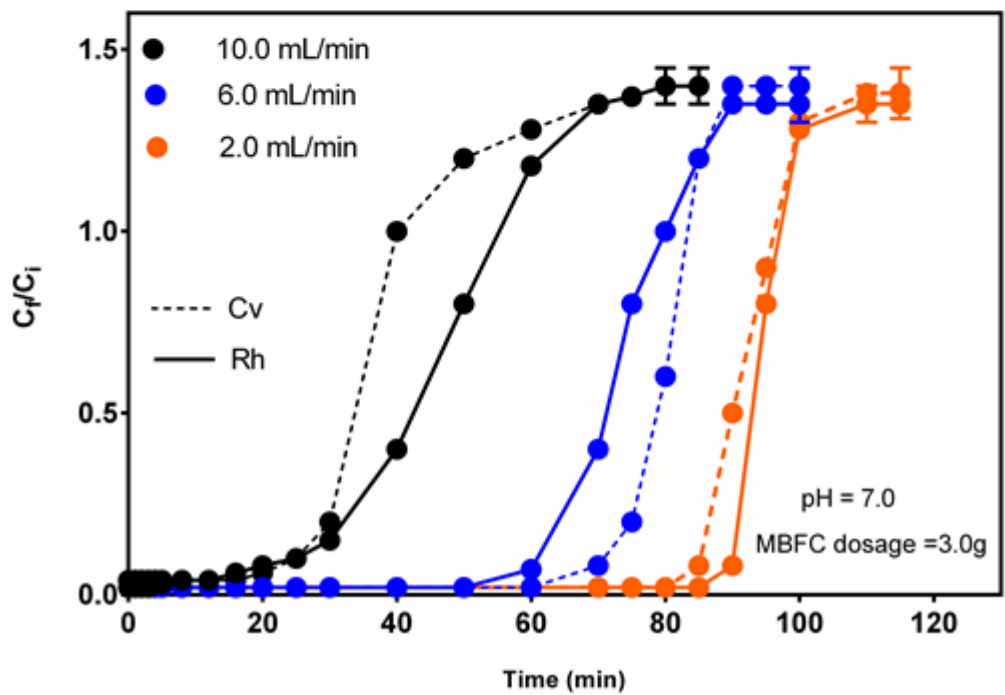
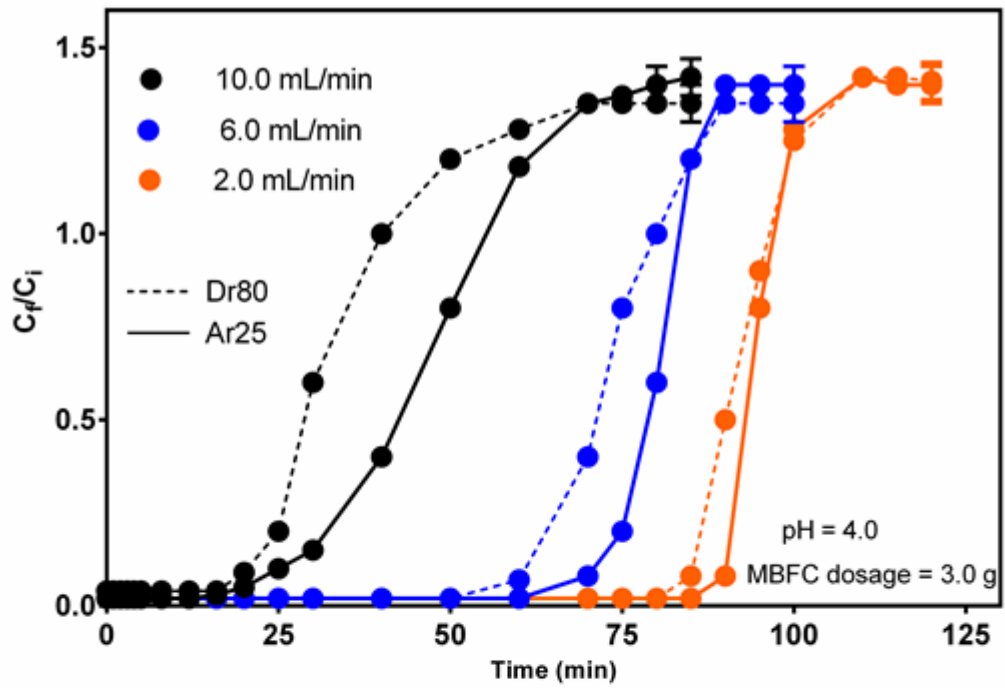


Figure 22: Effect of flow rate on dye removal in bed column of MBFC

4.5 Equilibrium Isotherm, Kinetics, and Sorption Thermodynamics

The effect of initial pollutants concentration was also assessed, and data obtained were fed into different isotherm models to understand the pollutant-adsorbent interaction through the suitability of the models. It was observed that the uptake capacity of the adsorbate increased drastically with an increase in adsorbate concentration when all other parameters held constant. This is ascribed to increasing driving force of the adsorbate concentration gradient and intense interaction with the sorption sites (Zhao et al., 2012). However, the percentage removal decreased with increasing concentration which is attributed to electrostatic competition between the adsorbate molecules for the finite active sites in the MBFC (Oladipo et al., 2015ab).

The adsorption data are fitted into the various isotherm models of each pollutant from binary and single component systems, omitting likely interaction from other solutes in the system. The relative and selectivity of the adsorbate in binary systems were further studied using the following equations:

$$\text{Relative adsorption } (R_{Ad}) = \frac{[q_c]_b}{[q_c]_s} \quad (13)$$

$$\text{Selectivity } (S_{Ad}) = \frac{[q_{c,1}]_b}{[q_{c,2}]_b} \quad (14)$$

where $[q_c]_b$, $[q_c]_s$, $[q_{c,1}]_b$ and $[q_{c,2}]_b$ denote the uptake capacity of specific pollutant in a binary system and single system at the same concentration, respectively. The parameters of the isotherm models obtained via the linear regression analysis are presented in Table 14.

Table 14: The isotherms parameters in single component system

Isotherms	Single Component System							
	Pollutants							
	Dr80	Ar25	Cv	Rh	Cu²⁺	Ni²⁺	Zn²⁺	Mn²⁺
Langmuir								
$q_{e,exp}$ (mgg ⁻¹)	301.3	372.3	233.8	333.4	232.5	289.7	285.4	298.3
q_m (mgg ⁻¹)	304.3	384.5	220.4	338.4	232.1	279.5	293.8	295.3
K_L (Lg ⁻¹)	34.98	31.78	38.99	45.98	42.78	54.11	45.22	54.89
R^2	0.828	0.845	0.989	0.999	0.995	0.993	0.997	0.991
Freundlich								
$q_{e,exp}$ (mgg ⁻¹)	301.3	372.3	233.8	333.4	232.5	289.7	285.4	298.3
k_f (Lg ⁻¹)	128.4	195.9	242.4	128.9	292.5	167.5	153.6	295.3
n	0.987	0.954	1.063	1.011	0.896	2.112	1.291	0.999
R^2	0.985	0.999	0.996	0.997	1.000	0.989	0.996	0.995
Sips								
$q_{e,exp}$ (mgg ⁻¹)	301.3	372.3	233.8	333.4	232.5	289.7	285.4	298.3
q_m (mgg ⁻¹)	139.5	211.9	104.9	234.9	98.5	109.5	145.8	100.3
K_s (min ⁻¹)	0.076	0.089	0.094	0.087	0.123	0.231	0.144	0.198
n_s	1.891	1.541	2.981	1.981	1.098	1.931	1.432	1.981
R^2	0.897	0.799	0.895	0.992	0.945	0.919	0.923	0.895
R–P								
K_{RP} (Lg ⁻¹)	0.091	0.098	0.561	0.781	0.456	0.981	0.331	0.467
a_{rp} (Lmg ⁻¹)	1.781	2.911	1.789	3.098	2.456	3.981	4.911	5.098
β	0.982	0.891	0.931	0.783	0.913	0.681	0.899	0.794
R^2	0.885	0.799	0.999	0.989	0.995	0.997	0.996	0.994

(MBFC dose: 100 mg, 500 mgL⁻¹ initial concentration and 200 rpm)

As indicated, the regression coefficients (R^2) in the single component for R–P and Langmuir isotherms are found to be closer to 1 for the basic dyes and the heavy metal ions. On the other hand, the Freundlich isotherm was observed to give a better correlation for the acidic dyes in the single component system. This observation suggests that the uptake of the basic dyes and heavy metal ions is via monolayer adsorption while those of acidic dyes occurred by multilayer sorption process.

Table 15: Isotherm parameters for binary component system

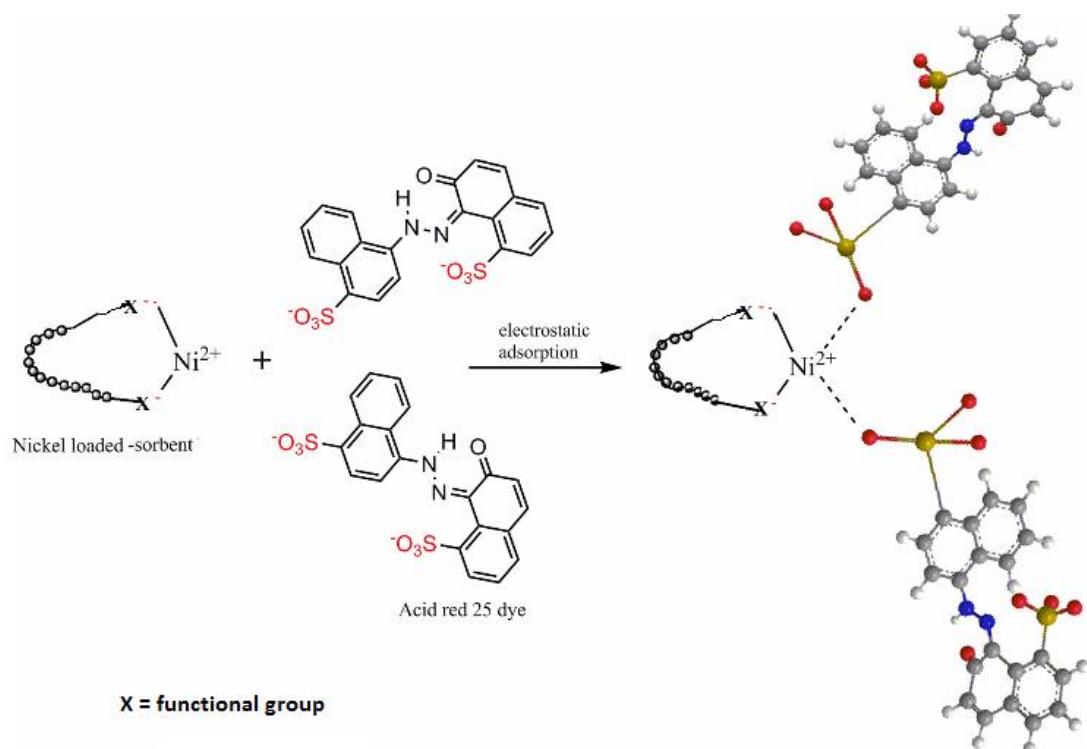
Isotherms	Binary Component System				
	Pollutants				
Langmuir	Dr80 + Ar25	Cv + Rh	Dr80 + Cu ²⁺	Cu ²⁺ + CV	Cu ²⁺ + Ni ²⁺
$q_{e,exp}$ (mgg ⁻¹)	235.9	182.4	158.5	133.8	142.8
q_m (mgg ⁻¹)	94.9	107.6	123.4	68.1	82.9
K_L (Lg ⁻¹)	33.1	22.9	23.8	32.8	23.9
R^2	0.887	0.901	0.861	0.888	0.910
Freundlich					
$q_{e,exp}$ (mgg ⁻¹)	235.9	182.4	158.5	133.8	142.8
k_f (Lg ⁻¹)	101.9	112.8	98.9	113.5	92.3
n	3.871	2.981	1.981	2.981	3.198
R^2	1.000	0.999	0.997	0.994	0.995
Sips					
$q_{e,exp}$ (mgg ⁻¹)	235.9	182.4	158.5	133.8	142.8
q_m (mgg ⁻¹)	211.8	189.5	163.4	130.6	145.9
K_s (min ⁻¹)	0.056	0.098	0.087	0.057	0.981
n_s	1.234	2.119	2.898	3.191	3.112
R^2	0.999	0.998	0.998	0.999	0.988
R-P					
K_{RP} (Lg ⁻¹)	0.093	0.092	0.663	0.581	0.656
a_{rp} (Lmg ⁻¹)	1.098	2.098	2.711	3.033	2.411
β	0.981	0.808	0.977	0.903	0.874
R^2	0.891	0.817	0.918	0.907	0.917
Relative Adsorption Capacity					
R_{ad}	0.98	0.48	1.23	0.67	0.89
Selectivity					
S_{ad} at pH 6.0	Dr80 > Ar25	Rh > Cv	Cu ²⁺ > Dr80	Cv > Cu ²⁺	Cu ²⁺ > Ni ²⁺

(Pollutants in binary mixture are of same concentration and MBFC dose: 100 mg)

It is important to stress that the Sips and Freundlich isotherms provide an acceptable fit for all the pollutant in a binary system (Table 15) and all values of n are greater than 1, indicating favorable adsorption conditions. Comparing the K_f of the acidic dyes in the single component system, the uptake capacity of MBFC for DR80 is much lower than that of Ar25, which is likely due to the lower molecular size of Ar25 (502 gmol⁻¹) as compared with that of Dr80 (1373 gmol⁻¹). The less bulky structure of Ar25 makes it easy to diffuse into MBFC core, and also Dr80 molecule has more sulfate groups that might interacted with more protonated functional groups

(hydroxyl or amine) on MBFC, thereby reducing its uptake. [Yan et al., 2014](#) had reported similar scenario for the uptakes of acid orange 7 and acid green 25 by chitosan-based composite beads.

It was reported that; if $R_{ad} > 1$, the uptake of pollutant “*i*” with same initial concentration was enhanced by the existence of co-pollutant; if $R_{ad} < 1$, the removal of pollutant “*i*” was inhibited by the co-pollutant and if $R_{ad} = 1$, the co-pollutant does not affect the removal of the pollutant “*i*” ([Deng et al., 2013](#); [Tover-Gomez et al., 2012](#)). The adsorption capacities involving the investigated basic dyes and heavy metal ions were reduced in the binary experimental studies, indicating the existence of steric hindrance and antagonistic adsorption process ([Deng et al., 2013](#)). However, the uptake of acidic dyes was enhanced in the presence of heavy metals ions, indicating synergistic adsorption. The reason for the enhancement may be explained by the fact that heavy metal ions adsorbed on the surface of MBFC interacted electrostatically with the incoming anionic dyes via the creation of new specific sorption sites as illustrated in [Scheme 2](#). [Tover-Gomez et al., \(2012\)](#) also reported synergic adsorption for the simultaneous of heavy metals and acid blue 25 using modified carbon-based composite.



Scheme 2: Schematic illustration of synergistic adsorption between nickel-loaded adsorbent and acid red 25

Furthermore, the adsorption selectivity of the adsorbates was assessed at the same concentration and the following sequence obtained; Dr80>Ar25, Rh>Cv, and Cu>Ni>Mn>Zn in the multicomponent systems. It is worth noting that variation in individual concentration in the multicomponent system may result in a different sequence, but such variation was not investigated in this thesis. However, we reported in our previous research the variation in copper and Dr80 initial concentrations in a binary system and detailed explanation presented in [Oladipo and Gazi, 2015a](#).

Table 16: Pseudo-first and pseudo-second-order kinetic parameters

Kinetic models		Single Component System							
		Pollutants							
Pseudo-first		Dr80	Ar25	Cv	Rh	Cu ²⁺	Ni ²⁺	Zn ²⁺	Mn ²⁺
	$q_{e,exp}$ (mgg ⁻¹)	328.9	402.6	298.6	403.4	292.5	189.7	165.9	198.6
	$q_{e,cal}$ (mgg ⁻¹)	204.8	327.1	120.8	208.1	132.9	178.4	193.2	245.8
	k_1 (min ⁻¹)	0.0034	0.0031	0.0045	0.0019	0.0031	0.0019	0.0056	0.0011
	$h_{0,1}$	0.279	0.349	0.756	0.654	0.345	0.423	0.612	0.239
	R^2	0.928	0.945	0.956	0.823	0.911	0.908	0.932	0.871
Pseudo-second									
	$q_{e,exp}$ (mgg ⁻¹)	328.9	402.6	298.6	403.4	292.5	189.7	165.9	198.6
	$q_{e,cal}$ (mgg ⁻¹)	331.8	407.4	300.8	408.9	292.9	187.4	173.6	195.3
	k_2 (g/mg min)	0.0065	0.0081	0.0063	0.0045	0.0065	0.0038	0.0088	0.0039
	$h_{0,2}$	0.222	0.149	0.351	0.453	0.545	0.123	0.312	0.208
	R^2	0.985	0.999	0.996	0.997	1.000	0.989	0.996	0.995
Kinetic models		Binary Component System							
		Dr80 + Ar25	Cv + Rh	Dr80 + Cu ²⁺	Cu ²⁺ + CV	Cu ²⁺ + Ni ²⁺			
Pseudo-first	$q_{e,exp}$ (mgg ⁻¹)	111.9	282.4	358.6	93.4	112.8			
	$q_{e,cal}$ (mgg ⁻¹)	104.3	277.5	360.4	98.1	122.9			
	k_1 (min ⁻¹)	0.0012	0.0022	0.0025	0.0013	0.0078			
	$h_{0,1}$	0.768	0.149	0.756	0.654	0.345			
	R^2	0.999	0.998	1.000	0.996	0.989			
Pseudo-second									
	$q_{e,exp}$ (mgg ⁻¹)	111.9	282.4	358.6	93.4	112.8			
	$q_{e,cal}$ (mgg ⁻¹)	234.8	127.4	125.9	128.4	162.6			
	k_2 (g/mg min)	0.0012	0.0023	0.0065	0.0027	0.0044			
	$h_{0,2}$	0.879	0.219	0.656	0.854	0.645			
R^2	0.889	0.988	0.913	0.907	0.954				

(MBFC dose: 100 mg, 500 mgL⁻¹ initial concentration and 200 rpm)

The parameters obtained from kinetic models fitting, and correlation coefficients are listed in Table 16. Higher correlation coefficients (greater than 0.985) were obtained from pseudo-second-order in a single component system than that from pseudo-first-order ($R^2 = 0.823 - 0.956$). However, pseudo-first-order is more favorable in the binary system, indicating that chemisorption controls the single component system while physical adsorption predominates in a binary system. Furthermore, the h values of the acidic dyes are much lower in a single component system than in the presence

of co-pollutants. This difference confirms that the adsorbed metal ions enhanced both the mass transfer and uptake capacity of the acidic dyes in the binary system which is technically consistent with the isotherms data.

Table 17: Parameters for intraparticle diffusion and Boyd mechanism

Intraparticle diffusion	Single Component System								
	Pollutants								
	Dr80	Ar25	Cv	Rh	Cu ²⁺	Ni ²⁺	Zn ²⁺	Mn ²⁺	
k_{d1} (mg/gmin ^{-0.5})	1.032	1.564	1.432	1.651	1.076	1.231	1.431	1.651	
k_{d2} (mg/gmin ^{-0.5})	1.236	1.981	1.651	1.891	1.231	1.321	1.618	1.981	
C_1	5.781	6.981	6.431	7.123	8.123	7.171	5.981	6.811	
C_2	3.211	4.981	5.971	3.981	5.981	5.981	3.981	4.981	
R^2	0.918	0.987	0.999	0.987	0.991	0.968	0.992	0.989	
Boyd	Binary Component System								
	Dr80 +Ar25	Cv+ Rh	Dr80 + Cu ²⁺	Cu ²⁺ + CV	Cu ²⁺ + Ni ²⁺				
	k_{d1} (mg/gmin ^{-0.5})	1.001	1.214	1.286	1.314	1.218			
	k_{d2} (mg/gmin ^{-0.5})	0.013	0.915	0.891	0.891	1.111			
	C_1	3.981	2.981	3.981	4.981	4.231			
	C_2	2.911	1.149	1.756	2.654	1.345			
	R^2	0.998	0.979	1.000	0.988	0.996			
	Single Component System								
	$D_c \times 10^5$ (cm ² /s)	1.98	1.49	1.89	0.99	0.65			
	R^2	0.987	0.999	0.987	0.998	0.976			
Binary Component System									
$D_c \times 10^5$ (cm ² /s)	1.87	1.98	0.82	0.87	0.45				
R^2	0.989	0.999	1.000	0.987	0.998				

(MBFC dose: 100 mg, 500 mgL⁻¹ initial concentration and 200 rpm)

Also, intraparticle diffusion may also partake in the sorption process, and the parameters obtained from the intraparticle diffusion equation are presented in Table 17.

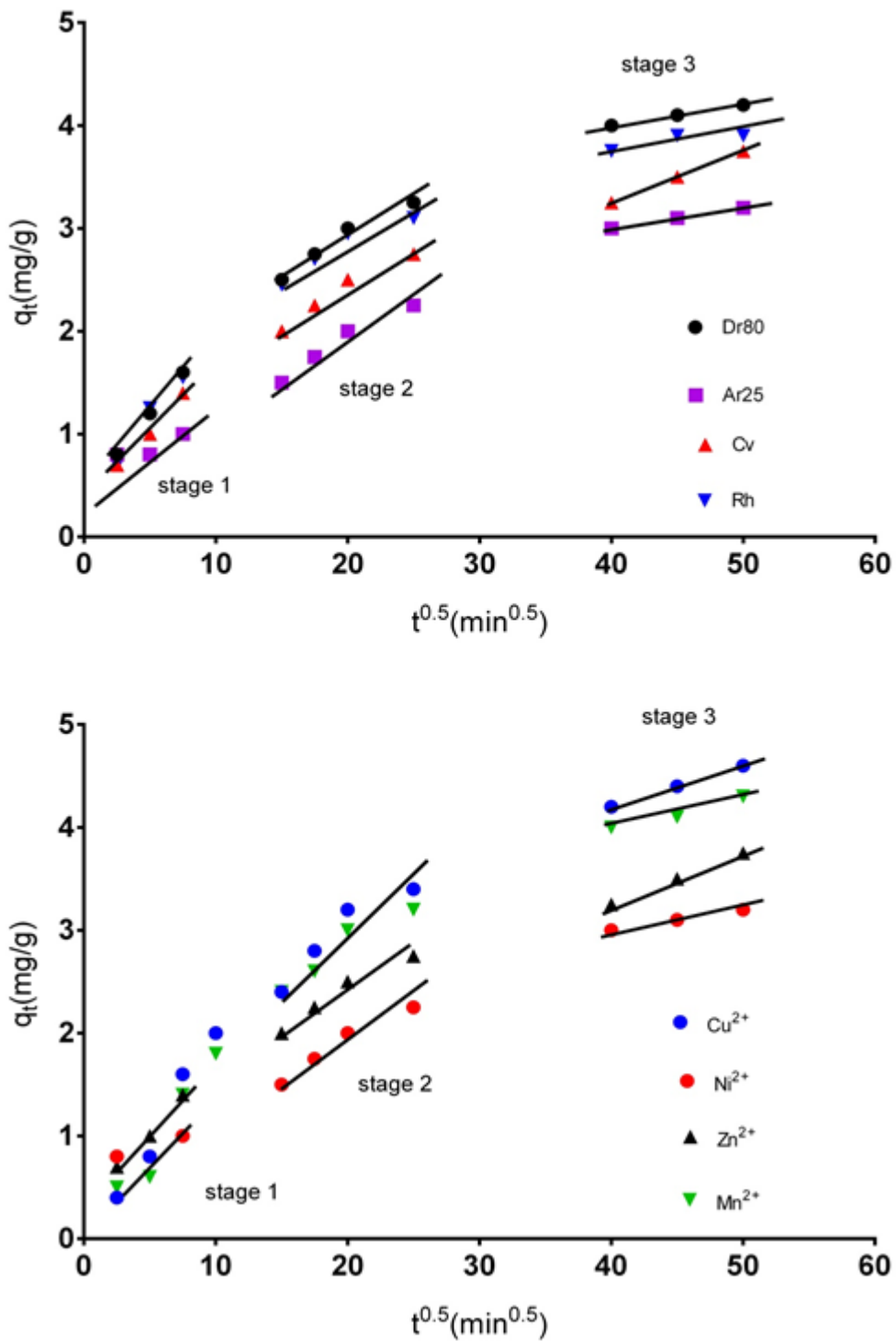


Figure 23: Plot of intraparticle diffusion of dyes and heavy metal ions

According to Yan et al., 2014, intraparticle diffusion would be the sole rate-controlling step if the plots pass through the origin. Otherwise, other mechanisms

may be involved. As seen in Fig. 23, the plots do not pass through the origin and three sorption steps were obtained, indicating the uptake was controlled by different sorption mechanisms. These steps can be explained as thus: **(a)** the initial sharp step shows mass transfer of the adsorbate molecules from bulk solution to the external surface of the MBFC, **(b)** the second stage is noted to be slower as compared to the first portion and it indicates gradual sorption process, which may be ascribed to intraparticle diffusion of unadsorbed molecules at the first stage and **(c)** the third stage denotes the final equilibrium attainment where the residual adsorbate concentration became distinctly low (Deng et al., 2013; Oladipo et al., 2014).

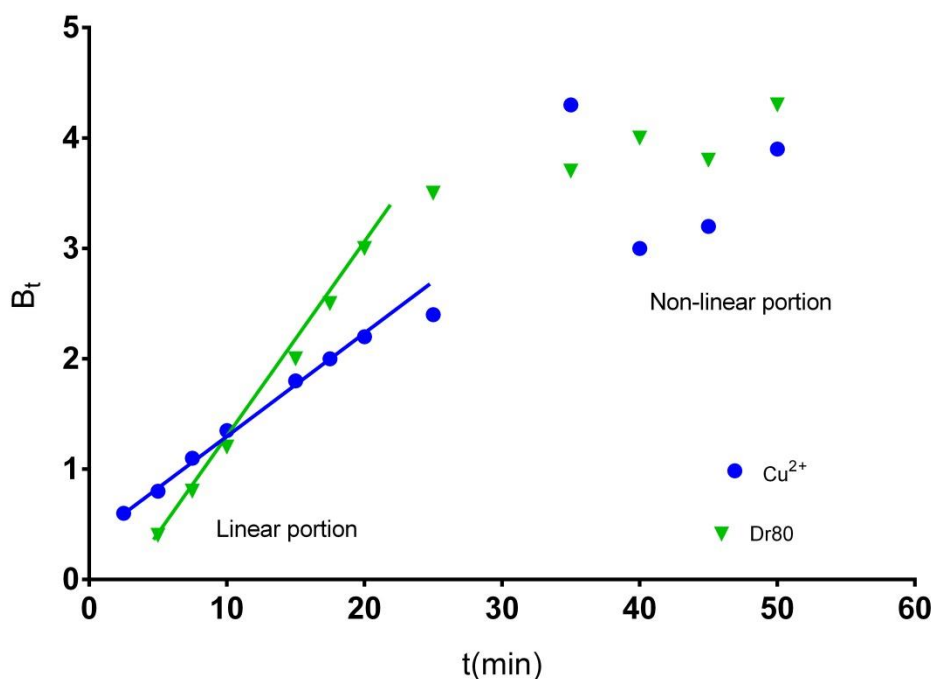


Figure 24: Boyd plots for Dr80 and Cu²⁺ removal by MBFC

To corroborate the actual rate controlling steps in the sorption of the investigated pollutants, the experimental data were further analyzed using Boyd equation and obtained plots are shown in Fig. 24. The plots did not pass through the origin and noted to be linear only at the early period of the sorption, confirming that external

mass transfer is the rate-controlling mechanism (Hameed and El-Khaiary, 2008). The effect of temperature on the sorption of the pollutants and thermodynamic analysis were performed.

The uptake capacity of MBFC is enhanced in a single component system with increases in temperature. The boundary layer effects become weakened as temperature increases; hence the higher temperatures enhance the diffusion of the pollutant molecules and subsequently increased the sorption rates. However, in binary system increases in temperature reduces the uptake capacity of the MBFC, confirming competitive adsorption due to insufficient sorption sites. The thermodynamic parameters reveal that the sorption process is feasible and spontaneous, and also the process is a combination of chemisorption and physical mechanisms (Table 18).

Table 18: Thermodynamic parameters in single and binary systems

Pollutants	T(K)	K_d	ΔH° (kJ/mol)	ΔS° (J/molK)	ΔG° (kJ/mol)
Single Component System					
Dr80	298	2.86	57.94	194.45	-2.60
	328	4.81			-4.28
Ar25	298	2.60	43.42	145.70	-2.37
	328	4.29			-3.97
Cv	298	2.25	42.78	143.55	-2.01
	328	2.49			-2.45
Rh	298	1.81	50.23	168.56	-1.47
	328	2.34			-2.32
Cu ²⁺	298	1.78	46.02	154.45	-1.43
	328	1.34			-0.80
Ni ²⁺	298	2.59	47.49	159.39	-2.36
	328	4.11			-3.85
Zn ²⁺	298	2.33	69.97	234.81	-2.11
	328	4.18			-3.9
Mn ²⁺	298	2.09	61.32	205.78	-1.83
	328	3.98			-3.77
Binary Component System					
Dr80 + Ar25	298	5.62	43.66	146.54	-4.28
	328	6.78			-5.22
Cv + Rh	298	4.98	54.89	184.22	-4.38
	328	5.33			-4.15
Cu ²⁺ + Ni ²⁺	298	3.98	74.59	250.33	-3.42
	328	4.99			-4.38
Dr80 + Cu ²⁺	298	3.11	53.34	178.99	-3.09
	328	5.44			-4.19
Cv + Ni ²⁺	298	2.98	55.59	186.56	-2.71
	328	3.87			-3.69

(MBFC dose: 100 mg, 50 mgL⁻¹ initial concentration, time: 480 min and 200 rpm)

4.6 Regeneration and Reuse Results

The efficiency and reusability of MBFC were further assessed by desorbing the loaded adsorbates and reusing of the spent MBFC in four cycles. To make the process economical, desorption experiments were conducted using three different

desorbing agents. About 75% desorption was obtained when NaOH was used; this can be explained by the fact that the hydroxyl ions could replace the loaded anionic dyes from the MBFC sorption sites. 85% desorption was obtained when HCl was used and 95.5% desorption obtained in the presence of ethanol mixture (Fig. 25). This observation was consistent with the report of Tu et al., 2014.

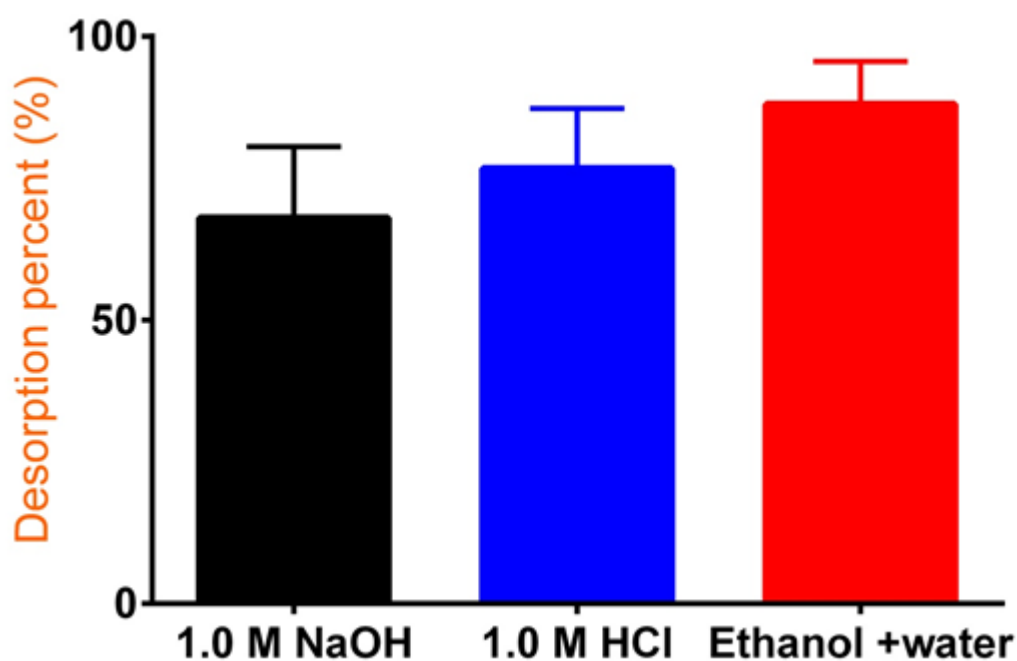


Figure 25: Desorption of loaded MBFC using different desorbing agents at 298K

The results from the reuse experiments revealed that MBFC is stable and efficient to be reused for uptake of various pollutants from effluents up to the fourth cycles (Fig. 26). As observed the uptake capacity of the spent MBFC decreased with increasing reuse cycles. A drastic change in the removal efficiencies was noticed after the third cycle; however, visual assessment of the spent composite indicated that MBFC had the potential for reusability in large-scale operations.

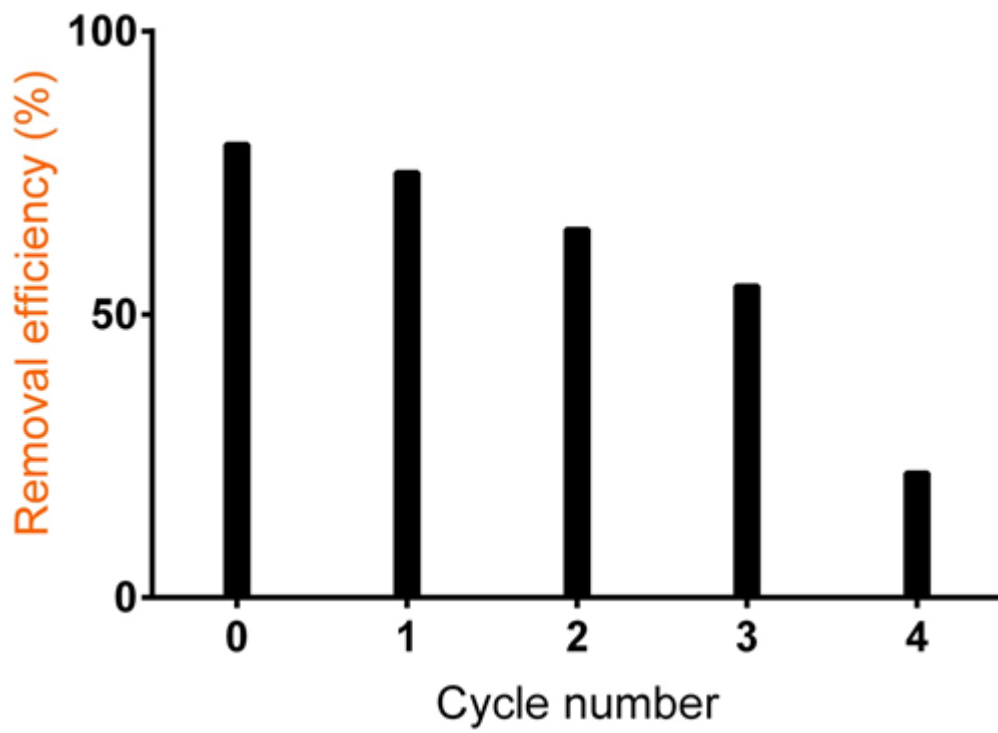


Figure 26: Reusability of MBFC

Chapter 5

CONCLUSION

In summary, various adsorbents were prepared for the simultaneous removal of acidic dyes (Dr80 and Ar25), basic dyes (Cv and Rh) and heavy metal ions (Cu^{2+} , Ni^{2+} , Zn^{2+} , and Mn^{2+}). Techno-economic optimization, adsorption isotherm, kinetic analysis, parametric and thermodynamic studies were performed. The following significant conclusions obtained:

- Eight adsorbents were prepared, characterized and utilized, however MBFC composite gave higher performance when the effect of pH was examined and was used for other experiments.
- Using the Box-Behnken approach, the optimum operation conditions of 50 mgL^{-1} initial adsorbate concentration, 100 mg MBFC dose, 360 min contact time, pH 4.0 (acidic dyes) and pH 7.0 (basic dyes and heavy metal ions) were obtained to yield maximum removal efficiencies of 69.3–96.9%.
- Using the central composite design method, the average operation costs obtained under optimum ambient conditions for removal of the dyes and the heavy metals are 3.07 and 4.98 ₺/m^3 , respectively.
- The removal efficiencies were observed to be influenced by the presence of foreign cations (Li^+ , Na^+ , and K^+), also increases with increasing MBFC dose, and decreasing initial pollutant concentration.
- Freundlich and Sips isotherms best describe the equilibrium data in the binary system and effective also for acidic dyes in the single component

system, signifying heterogeneous process between the adsorbates and MBFC. However, adsorption process in the single component for basic dyes and heavy metal ions fitted well with the Langmuir model, specifying monolayer mechanisms.

- The pseudo-first-order equation best describes the kinetic data in the binary system indicating physical adsorption. However, the theoretical data generated by pseudo-second-order equation in a single component are consistent with the experiment data. This indicates chemisorptive sorption process.
- The intraparticle diffusion mechanism played a significant role in the sorption process.
- Boyd equation confirmed that the sorption process is controlled by the combination of external diffusion, pore diffusion, and chemisorption mechanisms.
- Conclusively, MBFC is an efficient and suitable composite for the removal of various pollutants. The composite performance is attributed to its heterogeneous surface functional groups and stability under various operating conditions.

REFERENCES

- Acharya, J., & Sahu, J.N. (2009). Removal of lead (II) from wastewater by activated carbon developed from Tamarind wood by zinc chloride activation. *Chem. Eng. J.* 149, 249–262.
- Ahmad, A.A., & Hameed, B.H. (2010). Fixed-bed adsorption of reactive azo dye onto granular activated carbon prepared from waste. *J. Hazard. Mater.* 175, 298–303.
- Asfaram, A., Ghaedi, M., Goudarzi, A., & Rajabi, M. (2015). Response surface methodology approach for optimization of simultaneous dye and metal ion ultrasound-assisted adsorption onto Mn doped Fe₃O₄-NPs loaded on. *Dalton Trans.* 44, 14707–14723.
- Bleiman, N., & Mishael, Y. G. (2010). Selenium removal from drinking water by adsorption to chitosan–clay composites and oxides: batch and columns tests. *J. Hazard. Mater.* 183, 590–595.
- Cui, L., Wang, Y., Hu, L., Gao, L., Du, B., & Wei, Q. (2015). Mechanism of Pb (II) and methylene blue adsorption onto magnetic carbonate hydroxyapatite/graphene oxide. *RSC Adv.* 5, 9759–9770.
- Chaturanga, P.K.D., Priyantha, N., Iqbal, S.S., & Iqbal, M.C.M. (2013). Biosorption of Cr (III) and Cr (VI) species from aqueous solution by *Cabomba caroliniana*: kinetic and equilibrium study. *Environ. Earth Sci.* 70, 661–671.

- Chieng, H.I., Zehra, T., Linda, B.L.L., Priyantha, N., & Tennakoon, D.T.B. (2014). Sorption characteristics of peat of Brunei Darussalam IV: equilibrium, thermodynamics and kinetics of adsorption of methylene blue and malachite green dyes from aqueous solution. *Environ. Earth Sci.* 72, 2263–2277.
- Dabrowski, A. (1999). Adsorption and Its Applications in Industry and Environmental Protection, 1st ed. Amsterdam: Elsevier, 1–11.
- Demirbas, A. (2008). Heavy metal adsorption onto agro-based waste materials: a review. *J. Hazard. Mater.* 157, 220–229.
- Deng, J.H., Zhang, X.R., Zeng, G.M., Gong, J.L., Niu, Q.Y., & Liang, J. (2013). Simultaneous removal of Cd (II) and ionic dyes from aqueous solution using magnetic graphene oxide nanocomposite as an adsorbent. *Chem. Eng. J.* 226, 189–200.
- Duran, A., Monteagudo, J.M., & Amores, E. (2008). Solar photo-Fenton degradation of Reactive Blue 4 in a CPC reactor. *Appl. Catalysis B: Environ.* 80, 42–50.
- Farooq, U., Kozinski, J.A., Khan, M.A., & Athar, M. (2010). Biosorption of heavy metal ions using wheat based biosorbents—a review of the recent literature. *Bioresour. Technol.* 101, 5043–5053.
- Gengec, E., Ozdemir, U., Ozbay, B., Ozbay, I., & Veli, S. (2013). Optimizing dye adsorption onto a waste-derived (modified charcoal ash) adsorbent using

Box–Behnken and central composite design procedures. *Water Air Soil Pollut.* 224, 1751–1763.

Hameed, B.H., & El-Khaiary, M.I. (2008). Malachite green adsorption by rattan sawdust: Isotherm, kinetic and mechanism modeling. *J. Hazard. Mater.* 153, 701–708.

Imamoglu, M. (2013). Adsorption of Cd (II) ions onto activated carbon prepared from hazelnut husks. *J. Dispersion Sci. Technol.* 34, 1183–1187.

Kang, J., Li, H., Zheng, Y.M., Qu, J., & Chen, J.P., (2010). Systematic study of synergistic and antagonistic effects on adsorption of tetracycline and copper onto a chitosan. *J. Colloid Interf. Sci.* 344, 117–125.

Khosa, M.A., Shah, S.S., & Nazar, M.F. (2011). Application of micellar enhanced ultrafiltration for the removal of methylene blue from aqueous solution. *J. Dispersion Sci. Technol.* 32, 260–264.

Liu, H., Qing, B., Ye, X., Li, Q., Lee, K., & Wu, Z. (2009). Boron adsorption by composite magnetic particles. *Chem. Eng. J.* 151, 235–240.

Manal, W.K. (2009). Removal of heavy metals and dyes from wastewater. *American University of Sharjah Repository; Msc thesis.*

Oladipo, A.A., Gazi, M., & Saber-Samandari, S. (2014). Adsorption of anthraquinone dye onto eco-friendly semi-IPN biocomposite hydrogel:

Equilibrium isotherms, kinetic studies and optimization. 2014. *J. Taiwan Inst. Chem. Eng.* 45, 653–64.

Oladipo, A.A., & Gazi, M. (2014a). Enhanced removal of crystal violet by low cost alginate/acid activated bentonite composite beads: Optimization and modelling using non-linear regression technique. *J. Water Proc. Eng.* 2, 43–52.

Oladipo, A.A., & Gazi, M. (2014b). Nickel removal from aqueous solutions by alginate-based composite beads: central composite design and artificial neural network modelling. *J. Water Proc. Eng.* doi: 10.1016/j.jwpe.2014.12.002.

Oladipo, A.A., & Gazi, M. (2014c). Fixed-bed column sorption of borate onto pomegranate seed powder-PVA beads: a response surface methodology approach. *Toxicol. Environ. Chem.* 96, 837–848.

Oladipo, A.A., & Gazi, M. (2015a). Microwaves initiated synthesis of activated carbon-based composite hydrogel for simultaneous removal of copper (II) ions and direct red 80 dye: A multi-component adsorption system. *J. Taiwan Inst. Chem. Eng.* 47, 125–136.

Oladipo, A.A., & Gazi, M. (2015b). Two-stage batch sorber design and optimization of biosorption conditions by Taguchi methodology for the removal of acid red 25 onto magnetic biomass. *Korean J. Chem. Eng.* 32, 1864–1878.

- Oladipo, A.A., & Gazi, M. (2015c). Removal of rhodamine b and nickel using hydroxyapatite based composites. *Toxicol. Environ. Chem*; Accepted.
- Oladipo, A.A., Gazi, M., & Yilmaz, E. (2015a). Single and binary adsorption of azo and anthraquinone dyes by chitosan-based hydrogel: Selectivity factor and Box-Behnken process design *Chem. Eng. Res. Design* 104, 264–279.
- Oladipo, A.A., Abureesh, M.A., & Gazi, M. (2015b). Bifunctional composite from spent “Cyprus coffee” for tetracycline removal and phenol degradation: Solar-Fenton process and artificial neural network. *Int. J. Biol. Macromol.* doi: 10.1016/j.ijbiomac.2015.08.054.
- Pandiselvi, K., & Thambidurai, S. (2013). Synthesis of porous chitosan–polyaniline/ZnO hybrid composite and application for removal of reactive orange 16 dye *Colloids Surf. B: Biointerf.* 108, 229–238.
- Ruthven, D.M. (1984). Principles of adsorption and adsorption processes. Canada: John Wiley & Sons.
- Sadhukhan, B., Mondal, N.K., & Chattoraj, S. (2014). Biosorptive removal of cationic dye from aqueous system: a response surface methodological approach *Clean Techn. Environ Policy* 16, 1015–1025.
- Sezgin, N., Sahin, M., Yalcin, A., & Koseoglu, Y. (2013). Synthesis, Characterization and, the Heavy Metal Removal Efficiency of MFe_2O_4 (M= Ni, Cu) Nanoparticles. *Ekoloji.* 22, 89–96.

- Tovar-Gomez, R., Rivera-Ramirez, D.A., Hernandez-Montoya, V., Bonilla-Petriciolet, A., Duran-Valle, C.J., & Montes-Moran, M.A. (2012). Synergic adsorption in the simultaneous removal of acid blue 25 and heavy metals from water using a $\text{Ca}(\text{PO}_3)_2$ -modified carbon. *J. Hazard. Mater.* 199-200, 290–300.
- Tu, Y.J., You, C.F., Chang, C.K., Chan, T.S., & Li, S.H. (2014). XANES evidence of molybdenum adsorption onto novel fabricated nano-magnetic CuFe_2O_4 . *Chem. Eng. J.* 244, 343–349.
- Wang, J., & Chen, C. (2014). Chitosan-based biosorbents: modification and application for biosorption of heavy metals and radionuclides. *Bioresour. Technol.* 160, 129–141.
- Wasewar, K.L., Atif, M., Prasad, B., Mishra I.M. (2009). Batch adsorption of zinc on tea factory waste. *Desalination* 244, 66–71.
- Xu, D., Tan, X.L., Chen, C.L., & Wang, X.K. (2008). Adsorption of Pb (II) from aqueous solution to MX-80 bentonite: effect of pH, ionic strength, foreign ions and temperature. *Appl. Clay Sci.* 41, 37–46.
- Yan, Y., Xiang, B., Yi, X., Li, Y., & Jia, Q. (2014). Competitive adsorption of acid dyes from aqueous solution on diethylenetriamine-modified chitosan beads. *J. Appl. Polym. Sci.* 131, 41168–41177.

- Zhang, Y., Tang, X., & Luo, W. (2014). Metal removal with two biochars made from municipal organic waste: adsorptive characterization and surface complexation modeling. *Toxicol. Environ. Chem.* 96, 1463–1475.
- Zhang, W.X., Yan, H., Li, H.J., Jiang, Z.W., Dong, L., Kan, X.W., Yang, H., Li, A.M., & Cheng, R.S. (2011). Removal of dyes from aqueous solutions by straw based adsorbents: Batch and column studies. *Chem. Eng. J.* 168, 1120–1127.
- Zhao, B., Shang, Y., Xiao, W., Dou, C., & Han, R. (2014). Adsorption of Congo red from solution using cationic surfactant modified wheat straw in column model. *J. Environ. Chem. Eng.* 2, 40–45.
- Zhao, S., Zhou, F., Li, L., Cao, M., Zuo, D., & Liu, H. (2012). Removal of anionic dyes from aqueous solutions by adsorption of chitosan-based semi-IPN hydrogel composites. *Composites: Part B.* 43, 1570–1578.